Texas A&M University
Mechanical Engineering Department
Turbomachinery Laboratory
Tribology Group

RESPONSE OF AN OPEN ENDS SQUEEZE FILM DAMPER TO LARGE AMPLITUDE IMPACT LOADS

Research Progress Report to the TAMU Turbomachinery Research Consortium

TRC-SFD-01-2014
by

Luis San Andrés
Mast-Childs Tribology Professor
Principal Investigator

Sung-Hwa Jeung
Research Assistant

Ziam Ghaznavi
Undergraduate Assistant

May 2014

EXECUTIVE SUMMARY

RESPONSE OF AN OPEN ENDS SQUEEZE FILM DAMPER TO LARGE AMPLITUDE IMPACT LOADS

LUIS SAN ANDRES, SUNG-HWA JEUNG, & ZIAM GHAZNAVI MAY 2014

With higher power densities and improved efficiencies, modern rotating machinery is forcing rotor-bearing systems to operate at increasingly higher speeds. As a result, bearing supports experience large dynamic loads and must undergo significant rotary deflection. A Squeeze Film Damper (SFD), if well designed, can reduce synchronous vibration response and shaft bending as the system crosses its critical speeds. Thus, aircraft engine and high-speed compressor designers favor using SFD to provide flexibility in rotor bearing systems to lower transmitted forces on the bearing supports and dissipate mechanical energy induced by journal vibration, especially for rotor bearing systems operating at supercritical speed [1,2].

In 2014, large amplitude impact loads, up to ~20g (pk-pk), were exerted onto an existing SFD test bearing that replicates a commercial jet-engine configuration with a squirrel cage support. The test rig consists of elastically supported bearing with a damper section having single film land length L=1 inch, diameter D=5 inch, and radial clearances c=213 μm (8.4 mil). The short length SFD (L/D=0.2) design offers a distinct advantage by reducing overall weight and space.

In tests, an electromagnetic shaker delivers impacts along two lateral planes up to 3.2 kN to the test bearing and can produce a maximum bearing cartridge (BC) displacement equal to 93% of radial damper clearance. Squeeze film force coefficients were extracted from the system force coefficients identified from the unidirectional impact load tests while oil circulating through the damper.

The test results show that the SFD direct damping coefficients (C_{XX}, C_{YY}) moderately increase with increasing maximum BC displacement (Z) up to 55% damper clearance, after which they begin to grow more rapidly, i.e., Z/c>0.55. The added mass coefficients (M_{XX}, M_{YY}) steadily increase as the BC peak amplitude (Z) increase up to ~6 kg at Z/c=0.87. SFD direct stiffness coefficients (K_{XX}, K_{YY}) are less than 30% of structural stiffness (K_S) for all test conditions. In general, the test SFD cross-coupled coefficients

$(K, C, M)_{SFD}$ are at least one order of magnitude lesser than the direct coefficients and thus, considered negligible.

With increasing amplitude, the damping ratio does not grow as rapidly as SFD direct damping coefficients since significant amount of added mass limits the growth of the damping ratio.

Measured dynamic pressures in the film lands show that the lubricated film peak dynamic pressures increase with load applied.

Predictions based on the short length SFD formulas agree modestly well within the uncertainty range of experimentally identified force coefficients, however, the model either over predicts or under predicts the inertia coefficients due to the model not accounting for the three orifice feed holes.

Nomenclature

B	Bias variable uncertainty [%]
c	Nominal radial clearance [m]
$C_{\alpha\beta,\ (\alpha,\beta=X,Y)}$	Damping coefficients [N.s/m]
C_S	Remnant damping coefficient [N.s/m]
$C_L\omega$	Model curve fits
D	Journal diameter [m], R= ½ D
e_s	Static eccentricity (along 45^o) [m]
e_X, e_Y	Dynamic eccentricity components [m]
f_n	Test system Natural frequency [Hz]
f_{start} ,f_{end}	Start and end frequencies for system parameter identification [Hz]
$H_{\alpha\beta,\ (\alpha,\beta=X,Y)}$	Test system impedances [N/m]
i	$\sqrt{-1}$. Imaginary unit
$K_{\alpha\beta,\ (\alpha,\beta=X,Y)}$	Stiffness coefficients [N/m]
K_S	Structural support stiffness [N/m]
L	Film land length [m]
$M_{\alpha\beta,\ (\alpha,\beta=X,Y)}$	Mass coefficients [kg]
$F_{\alpha(t),\ (\alpha=X,Y)}$	Dynamic force [N]
M_S	Remnant mass coefficients [kg]
M_{BC}	Bearing cartridge mass [kg]
P	Dynamic pressures in film land [Pa]
P_a	Ambient pressure [Pa]
P_{in}	Static oil pressure at journal inlet [Pa]
p-p	Peak to peak dynamic film pressures [Pa]
Q_{in}	Lubricant flow rate [LPM]
Q_T, Q_B	Lubricant flow rate through top and bottom lands [LPM]
r, r_X, r_Y	Circular orbit amplitude and its components along X and Y directions [m]
R	Journal radius [m], R= ½ D
R_T, R_B, R_o	Top and bottom film lands and orifice fluidic resistances
t	Time [s]
T	Temperature [ºC]
U_α	Total variable Uncertainty [%]
X,Y	Coordinate axes
$x_{(t)}$, $y_{(t)}$	Relative displacement of BC respect to the journal along X and Y direction [m]
Z	Maximum bearing cartridge displacement [m]
τ_d	Damped period [-]
α_v	Oil viscosity coefficient [1/ ºC]
ε	e_S/c. Dimensionless eccentricity [-]
ξ	Damping ratio [-]
δ	Logarithmic decrement [-]
ρ,μ	Oil density [kg/m^3] and viscosity [Pa.s]
ω	Excitation frequency [rad/s]

Vectors and matrices

$\mathbf{a}_{(t)}$	$\{a_X, a_Y\}^T$ Vector of bearing accelerations [m/s^2]
$\mathbf{C}$	Matrix of damping coefficient
$\mathbf{K}$	Matrix of stiffness coefficient
$\mathbf{F}_{(t)}$	$\{F_X, F_Y\}^T$ Vector of dynamic loads [N]
$\mathbf{H}$	$\mathbf{K} - \omega^2\mathbf{M} + i\,\omega\mathbf{C}$. Matrix of impedance coefficients [N/m]
$\mathbf{M}$	Matrix of added mass coefficient
$\mathbf{z}_{(t)}$	$\{x,y\}^T$ Vector of bearing displacements relative to journal [m]

Subscripts

BC	Bearing cartridge
k	Single frequency excitation index
s	Structure
L	Lubricated system
SFD	Squeeze film damper

TABLE OF CONTENTS

RESPONSE OF AN OPEN ENDS SQUEEZE FILM DAMPER TO LARGE AMPLITUDE IMPACT LOADS

LUIS SAN ANDRES, SUNG-HWA JEUNG, & ZIAM GHAZNAVI MAY 2014

LIST OF TABLES

LIST OF FIGURES

Introduction

Tubomachinery can often be subjected to multiple shock load excitations. Aircraft gas turbines, for example, inevitably experience sudden impact loads during hard landings and severe takeoffs [3,4]. Power plant turbines also experience seismic excitations, a typical example of low frequency base excitation. Excessive displacements can lead to system failure due to hard collision contact between a rotor and its bearings. Hence, accurate evaluation of the dynamic performance of rotor-bearing systems under operating conditions with external sudden dynamic loads forms the basis for sound mechanical design.

Squeeze File Dampers (SFDs) are customarily used in turbomachinery such as compressors and turbines, because of their ability to dissipate mechanical energy from rotor vibration, and to isolate structural components. Thus, SFDs improve the overall dynamic stability of rotor-bearing systems.

Since the mid-1980s, the SFD research program at Texas A&M University brings significant contributions to the development of improved SFD analysis and design tools benchmarked by SFD test data. Present work focuses on measuring the dynamic forced performance of a SFD under severe operating conditions (blade loss event) in ultra-short SFD (length to diameter ratio, L/D=0.2).

This technical report includes the identification of force coefficients, the assessment of the recorded film dynamic pressures, comparisons with predictions from the short length SFD model, and a discussion on the damping ratio for the lubricated test SFD system.

Test rig description

The annual report TRC-SFD-01-2013 [5] describes the test rig configuration. Figure 1 shows a picture of the current SFD test rig with its major components labelled. Figure 2 shows an isometric and top-down view of the test rig model with its major components. Two electromagnetic shakers are positioned orthogonally along the noted X and Y directions. A static loader positioned halfway between the two shakers, 45° away, apply static loads to displace the test bearing to a desired static eccentricity (e_s).

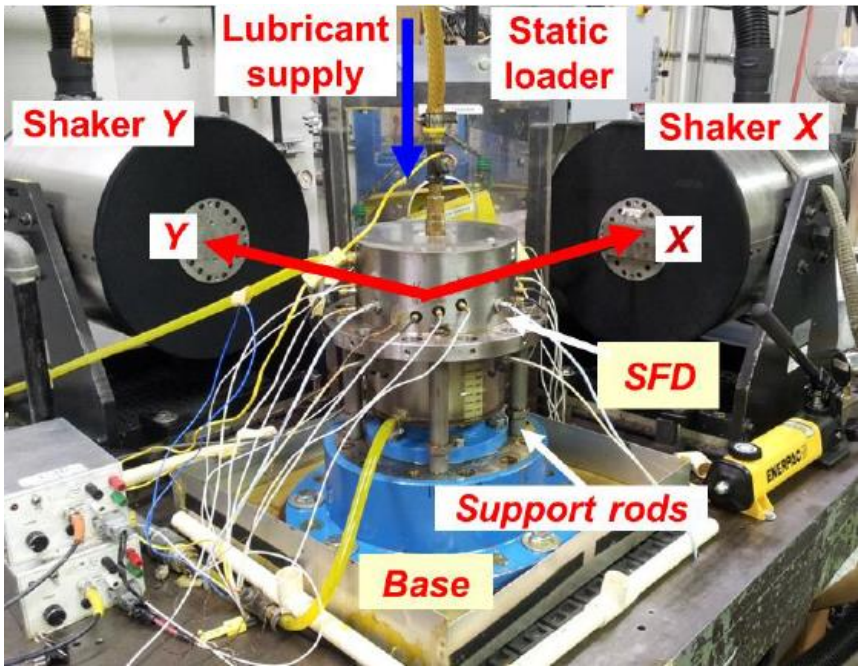

Figure 1. Picture of SFD test rig with shakers, static loader, and oil supply line

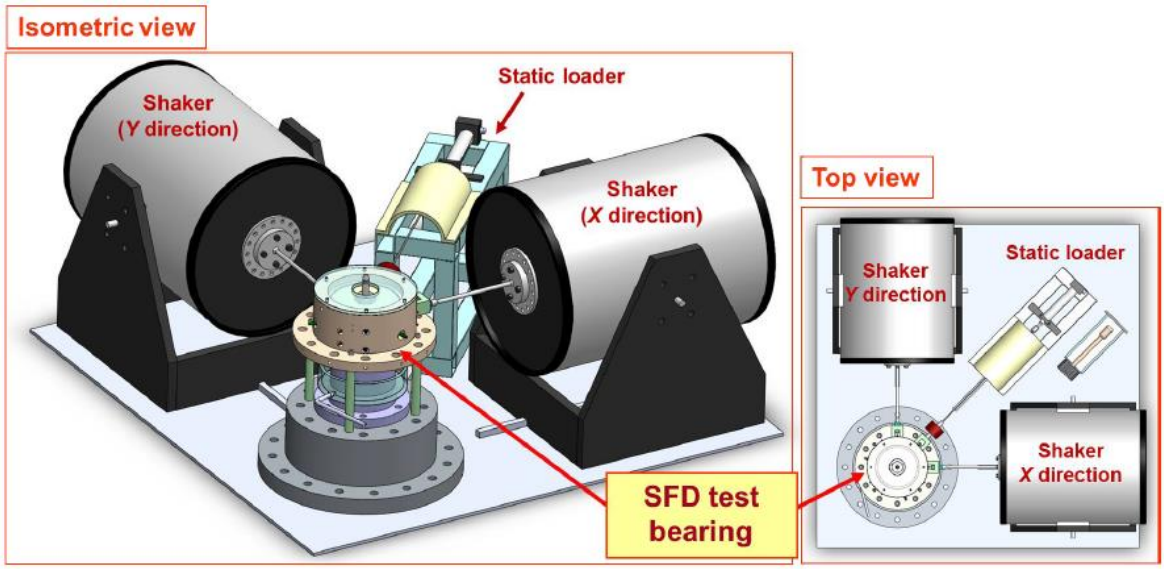

Figure 2. Isometric and top view of SFD test rig [5]

Figure 3 shows a cross-sectional view of SFD test rig and Table 1 lists the current damper geometry and lubricant properties. The journal is bolted directly to the base, whereas the bearing cartridge (BC) is supported by four main rods , spaced 90º apart, that connect to the base. All components are securely fastened to the iron test stand table. The BC provides an interface with the shakers and the static loader, and also holds various

sensors: two pairs of eddy current displacement sensors, two accelerometers, two load cells and six pressure sensors. This design allows the journal to be exchangeable without altering the bearing assembly and installed instrumentation.

As seen in Figure 3, the film land is created by the gap between the outer surface of the journal and the inner surface of the BC. The SFD consists of a single film land with length L=2.54 cm (1 inch), nominal diameter D=12.7 cm (5 inch), and a nominal radial clearance c=213 μm (8.4 mil). **Appendix A** details the measurement of the components' dimensions.

Lubricant (ISO VG2) is supplied through three radial holes (spaced 120° apart) wetting the film land and then discharging to ambient at the top and bottom sections. Oil collectors catch the oil and allow a return pump to move the oil back to a reservoir tank. As shown in the section A-A of Fig. 3, one of the feedholes is positioned 45° away from the X and Y axes.

The flow rate into the damper is set at Q_{in}= 4.5 LPM (1.2 GPM) and the lubricant supply pressure (P_{in}) measured upstream of the feedholes is maintained at 0.4 barg (5.5 psig). **Appendix B** details the measurement of lubricant properties (μ, ρ) and flow characteristics (P_{in}, Q_{in}).

Note that four structural rods support the bearing cartridge (BC) with mass M_{BC}=15.15 kg. The support structure lateral stiffness is K_s~10.9 MN/m. Note that the number of flexural support rods can be varied to change the structural stiffness of the rig.

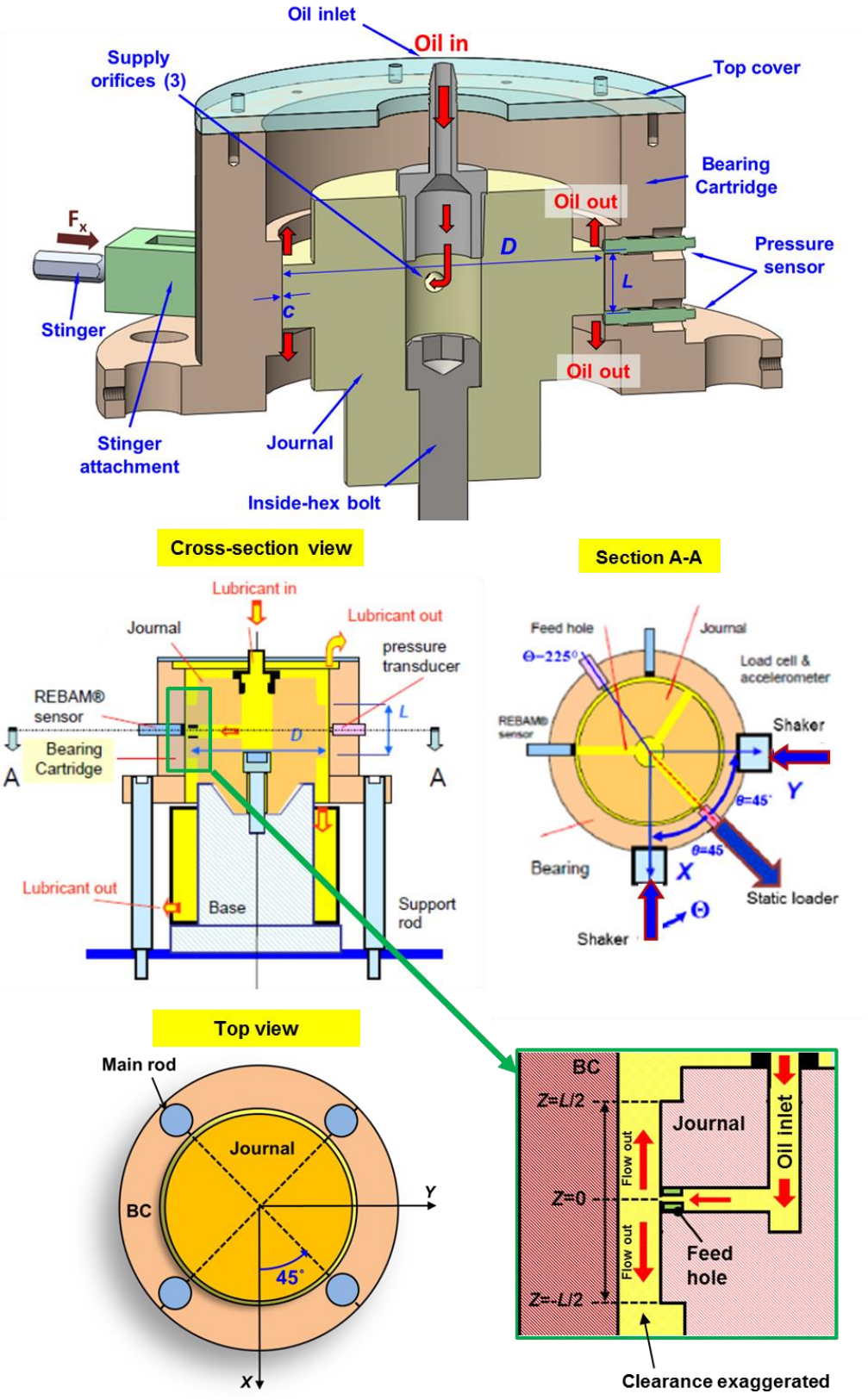

Figure 3. Schematic views of SFD test rig with physical dimensions and lubricant flow path (*L*=25.4 mm, *D*=126.7 mm, *c*=213 mil) [5].

Table 1. Open ends SFD geometry and oil properties

Journal diameter (D)	126.7 mm [4.9865 in]
Nominal radial clearance (c)	[213 ± 8 μm] 8.4 ± 0.3 mil
Film land length (L)	25.4 mm [1.0 in]
Three feed holes, diameter	2.57 mm [0.101 in] (120^o apart)
BC mass (M_{BC})	15.15 kg [33.40 lb]
ISO VG 2 viscosity (μ)	2.6 cP @ T_s 23 °C [0.377 micro-Reyns @ T_s=73°F]
ISO VG 2 density (ρ)	800 kg/m^3 [49.9 lb/ft^3]

Figure 4 shows a steel rod stinger attached to an e-shaker that delivers an impact force onto the test bearing. The AISI 1018 slender stinger has a flat surface at the striking end covered with an insulation tape. Note that the stingers are not affixed rigidly to the BC, but facing a pair of load cells located at the center of mass of the BC. In other words, the stinger merely pushes on the BC. A load cell aligned with a stinger records the dynamic force ($F_{X(t)}$ or $F_{Y(t)}$) from the shakers. Two accelerometers attached to the BC measure the absolute acceleration ($a_{X(t)}$, $a_{Y(t)}$) of the test bearing, and two REBAM® eddy current displacement sensors, installed in the BC and facing the stationary journal, measure the relative displacement ($Z_{X(t)}$, $Z_{Y(t)}$) of the BC.

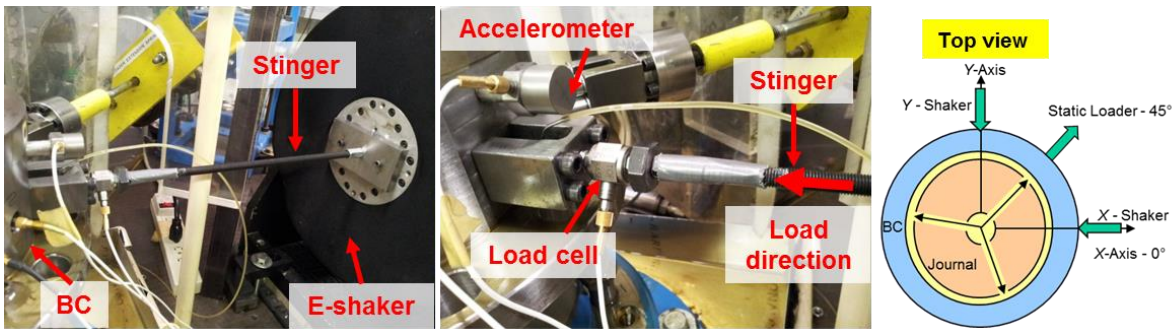

Figure 4. View of stinger connection to a shaker and instrumentation set up

Experimental procedure

Identification of the SFD dynamic force coefficients $(\mathbf{K}, \mathbf{C}, \mathbf{M})_{SFD}$ calls for a multiple step procedure. First, the test system structural stiffness ($\mathbf{K_s}$), damping ($\mathbf{C_s}$), and residual mass ($\mathbf{M_s}$) are estimated by performing static load tests and circular orbit tests[1] with the damper free of lubricant. Note, the circular orbit amplitude is 4% of the nominal damper clearance (r/c=0.04); hence it is sufficient for identifying the *true* (linearized) structure force coefficients[2].

The Instrumental Variable Filter Method (IVFM) [4] identifies the system force coefficients from the measurements of flexibility functions ($G_{\alpha\beta,\alpha\beta=X,Y}$) versus excitation frequency.

Appendix C describes the experimental procedure and identified system structural parameters over a frequency range of 10 – 250 Hz. In brief, the averages of the direct force coefficients are K_s=10.5 MN/m, C_s=1.0 MN/m, and M_s=2.0 kg. The estimated damping ratio (ζ) is ~4%, which is typical of a steel structure. The mass of the BC (14.65 kg) plus the effective mass contributed by the support rods (0.5 kg) is hereby referred to as the BC mass M_{BC} =15.15 kg[3]. The identified structural (dry) force coefficients $(\mathbf{K}, \mathbf{C}, \mathbf{M})_S$ are referenced as the '*baseline*' parameters.

Second, the sets of sudden impact tests performed with light lubricant (ISO VG 2) flowing through the damper film land yield the dynamic forced coefficients $(\mathbf{K}, \mathbf{C}, \mathbf{M})_L$ of the test damper. A series of ten impacts are delivered to the bearing cartridge assembly along the X direction. The data acquisition system records the applied force ($F_{X(t)}$) and ensuing relative displacement with respect to the stationary journal ($Z_{X(t)}$) and acceleration of the BC ($a_{X(t)}$). An in-house MathCAD code takes the recorded physical data of 10 impacts and averages them in the frequency domain. SFD force coefficients are identified from the frequency domain averages of ten impact forces and the respective bearing motion responses[4].

---

[1] For circular orbit tests, the stingers are connected to the bearing cartridge.

[2] A linearized force coefficient indicates an infinitesimally small displacement (ΔX) resulting from a change in force (ΔF), i.e., $K = \partial F / \partial X = \lim_{\Delta X \to 0} \Delta F / \Delta X$.

[3] The BC mass was measured on a scale prior to installation. Based on a structural beam calculation, M_{rods} is equivalent to the 25% the total mass of all four rods.

[4] Note that averaging the system responses assumes that the system response is linear with applied load.

For a sudden dynamic load (impact) test along the *X* axis, dynamic loads are applied at the *X* axis only whereas no load is imposed on the BC along the *Y* axis. Note the duration of the impact is approximately Δt_{imp}=1.7 ms. After the tests are completed, identical tests are performed with impact loads along the *Y*-direction. Therefore, the two load vectors are linearly independent

$$\mathbf{F}_X = \begin{bmatrix} F_{X_{(t)}} \\ 0 \end{bmatrix}; \quad \mathbf{F}_Y = \begin{bmatrix} 0 \\ F_{Y_{(t)}} \end{bmatrix} \tag{1}$$

The equation of motion for the test system supplied with lubricant and excited by the shaker external forces $\mathbf{F}_{(t)}$ is

$$M_{BC}\,\mathbf{a} + \mathbf{M_L}\ddot{\mathbf{z}} + \mathbf{C_L}\dot{\mathbf{z}} + \mathbf{K_L}\mathbf{z} = \mathbf{F} \tag{2}$$

where $\mathbf{K_L} = \mathbf{K_S} + \mathbf{K_{SFD}}$, $\mathbf{C_L} = \mathbf{C_S} + \mathbf{C_{SFD}}$, and $\mathbf{M_L} = \mathbf{M_S} + \mathbf{M_{SFD}}$. $\mathbf{F}=(F_X,\ F_Y)^{\mathrm{T}}$ is the load vector of the forces imposed on the BC, and $\mathbf{a}=(a_X,\ a_Y)^{\mathrm{T}}$ is the vector of the BC acceleration measured from the accelerometers, attached in the BC along the *X* and *Y* directions. $\mathbf{z}=(Z_X,\ Z_Y)^{\mathrm{T}}$ is the vector of relative displacements between the BC motion and the stationary journal.

Transforming the time domain equation of motions (3) into the frequency domain using discrete Fourier transform renders

$$\left(\mathbf{K_L} - \omega^2\mathbf{M_L} + i\omega\mathbf{C_L}\right)\bar{\mathbf{z}}_{(\omega)} = \bar{\mathbf{H}}_{(\omega)}\bar{\mathbf{z}}_{(\omega)} = \left(\bar{\mathbf{F}}_{(\omega)} - \omega^2 M_{BC}\,\bar{\mathbf{a}}_{(\omega)}\right)\bar{\mathbf{z}}_{(\omega)} \tag{3}$$

The SFD force coefficients are obtained by subtracting the dry system coefficients from the lubricated system coefficients:[5]

$$(\mathbf{K},\mathbf{C},\mathbf{M})_{\text{SFD}} = (\mathbf{K},\mathbf{C},\mathbf{M})_{\text{L}} - (\mathbf{K},\mathbf{C},\mathbf{M})_{\text{S}} \tag{4}$$

It is important to note that the identification procedure delivers parameters $(\mathbf{K}, \mathbf{C}, \mathbf{M})_{\text{SFD}}$ that are constant and valid within a (selected) frequency range.

[5] Equation 4 assumes the mechanical system is linear, i.e., the superposition principle is valid.

Identification of lubricated damper system parameter

Six sets of sudden dynamic (impact) load tests were performed with open ends single land SFD of radial clearance (c=213 μm) for increasing load amplitudes (0.5 - 3.2 kN) at the centered condition (e_s=0.0c).

Table 2 lists the range of amplitude dynamic forces and ensuing peak amplitude of BC. A series of ten impacts were delivered for each set of test. Note the signals from the instrumentation are stored as voltages over a given time span (1 sec) and the stinger struck the BC once very second.

Table 2. Test operating conditions for open ends SFD (c=213 μm)

Motion Type	Number of impacts	Max. load amplitude, F (kN)	Peak amplitude, Z (μm)
Unidirectional	10	0.5 - 3.24	39 - 196

Figure 5 depicts the maximum applied dynamic loads and ensuing maximum BC displacements (Z). Clearly, larger amplitude loads are needed to induce larger BC amplitudes. For a set of similar dynamic loads, the BC displaces more along the X direction than in the Y direction. The difference in structural stiffness along the X axis (K_{sXX}=10.6 MN/m) is ~5% smaller than the that of Y axis (K_{sYY}=11.1 MN/m) (see **Appendix C** for all identified structural parameters).

Figure 6 depicts the time trace of a typical impact load delivered to the BC and ensuing bearing displacement and acceleration along the X and Y directions, respectively. The data corresponds to a unidirectional impact load F_X=2.0 kN with maximum BC amplitude $|Z_X|_{Max}/c$=0.55. The electromagnetic shaker delivers a half-sine wave (impact) load and the impact force continues in time (duration) approximately 1.7ms. The ensuing response of the system is characterized as oscillatory with an exponentially decaying amplitude. The time responses of the BC (displacement and acceleration) die within 0.25 sec in the directions of impact. Notice the large acceleration approximately ~15 g (pk-pk).

BC motions orthogonal to the directions of impact are one order magnitude smaller than the BC response in the direction of impact; thus, not shown for brevity. Impact load test is measured in the step of 1 Hz at a rate of 4,096 samples/sec, Thus, the number of saved samples at discrete time intervals equals to 4,096.

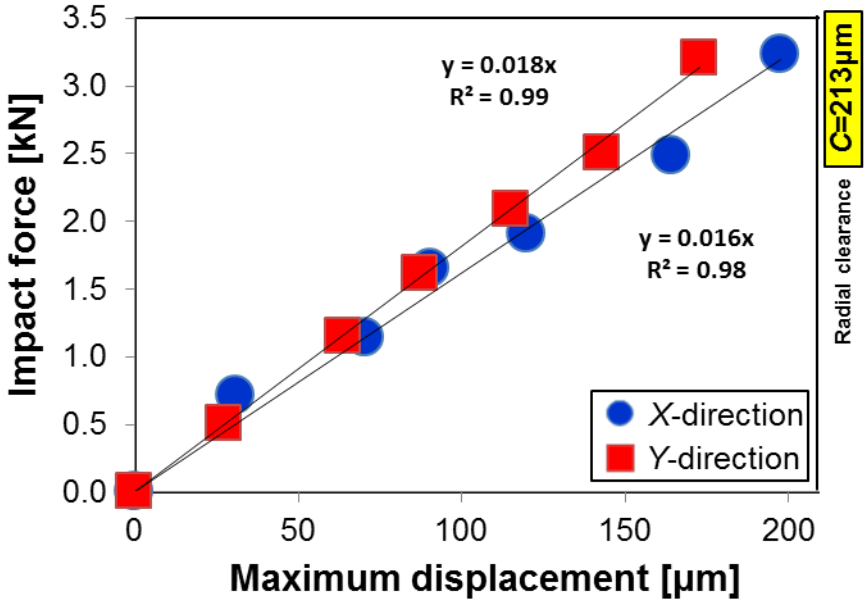

Figure 5. Maximum amplitude of dynamic load versus ensuing maximum displacement $\left|z_{X,Y}\right|_{Max}$ of the bearing cartridge. Open ends SFD nominal clearance *c*=213 μm.

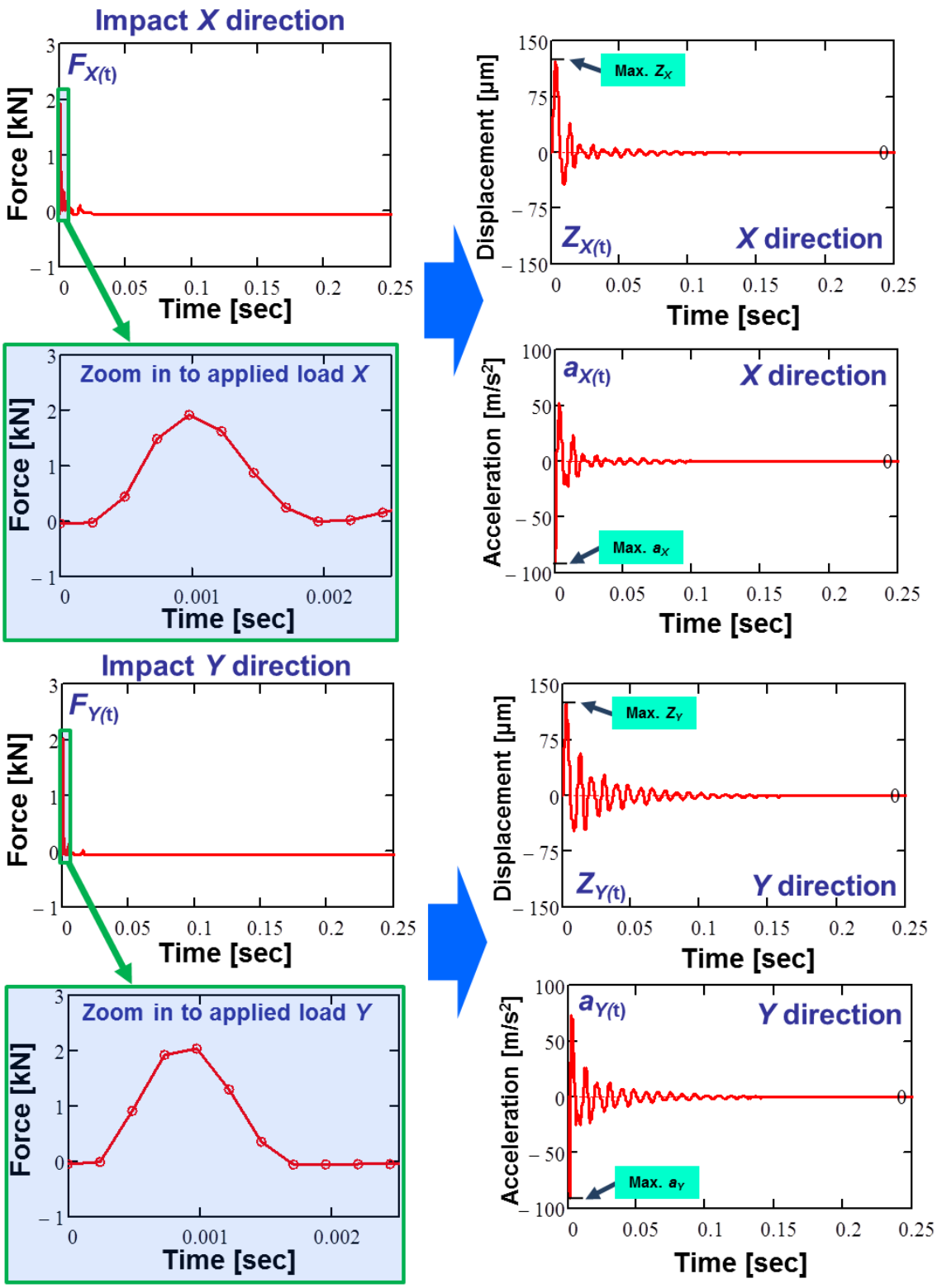

Figure 6. Typical impact loads, displacements and accelerations along *X* and *Y* directions (impact load tests) versus time. Lubricated and open ends SFD.

Figure 7 presents the real part of the lubricated system impedances, Re(H), and the respective physical model curve fits over the frequency range f_{start}=10 Hz to f_{end}=300 Hz. Note that the impedance matrix $\mathbf{H} = [\mathbf{K_L} - \omega^2 \mathbf{M_L} + i\omega \mathbf{C_L}]$ [6]. The test data correspond to dynamic impact loads (0.5 - 3.2 kN) and ensuing BC amplitudes (39 -196 μm). Recall that an experiment consists of ten impacts along each direction (X and Y) that are averaged in the frequency domain.

Re(H) shows high correlation factors (R^2 > 0.90) indicating the goodness fit between the data measured and physical model. With increasing BC amplitudes, Re(H) shows an increasing downward slope, $\text{Re}(H) \cong (K_s + K_{SFD}) - \omega^2 (M_s + M_{SFD})$, implying a increasing added mass M_{SFD}.

Note that data within frequencies from 130-190 Hz are excluded from the identification procedure. This is because the test rig pedestal has a natural frequency in this region causing an artificial "stiffening" of the test system. The data shows a large shift in measured impedances resulting in poor correlation between a model and the measured data in the range of 130-190 Hz [6].

Figure 8 depicts the imaginary part of the impedance, Im(H), and the model curve fits ($C_L\omega$) over the frequency range 10 - 300 Hz. The imaginary part shows the slopes that tend to increase with increasing BC amplitudes, thus evidencing that the direct damping coefficient is a function of the BC amplitude (r).

Test data and model showed the largest degree of correlation when only considered up to a cut-off frequency of 300 Hz. However, the test data for large (peak) BC displacement Z/c>0.42 and at high frequencies ω>250 Hz show scatter without a definite trend as the impact force clearly does not excite high frequency components.

Appendix D shows the real and imaginary parts of the direct (H_{XX}, H_{YY}) and the cross-coupled (H_{XY}, H_{YX}) dynamic impedances obtained from the small to large amplitude load tests (0.5 - 3.2 kN) and ensuing BC amplitudes (39 -196 μm). Overall, the real and imaginary parts of cross-coupled dynamic impedances, Re(H_{XY}) and Im(H_{XY}), are more than one order of magnitude smaller than the corresponding Re(H_{XX}) and Im(H_{YY}). Expectedly, Re(H_{XY}) and Im(H_{XY}) show low correlation factors (R^2) relative to the physical model.

[6] Lubricated force coefficients $(K, C, M)_L$ also include structure force coefficients $(K, C, M)_S$.

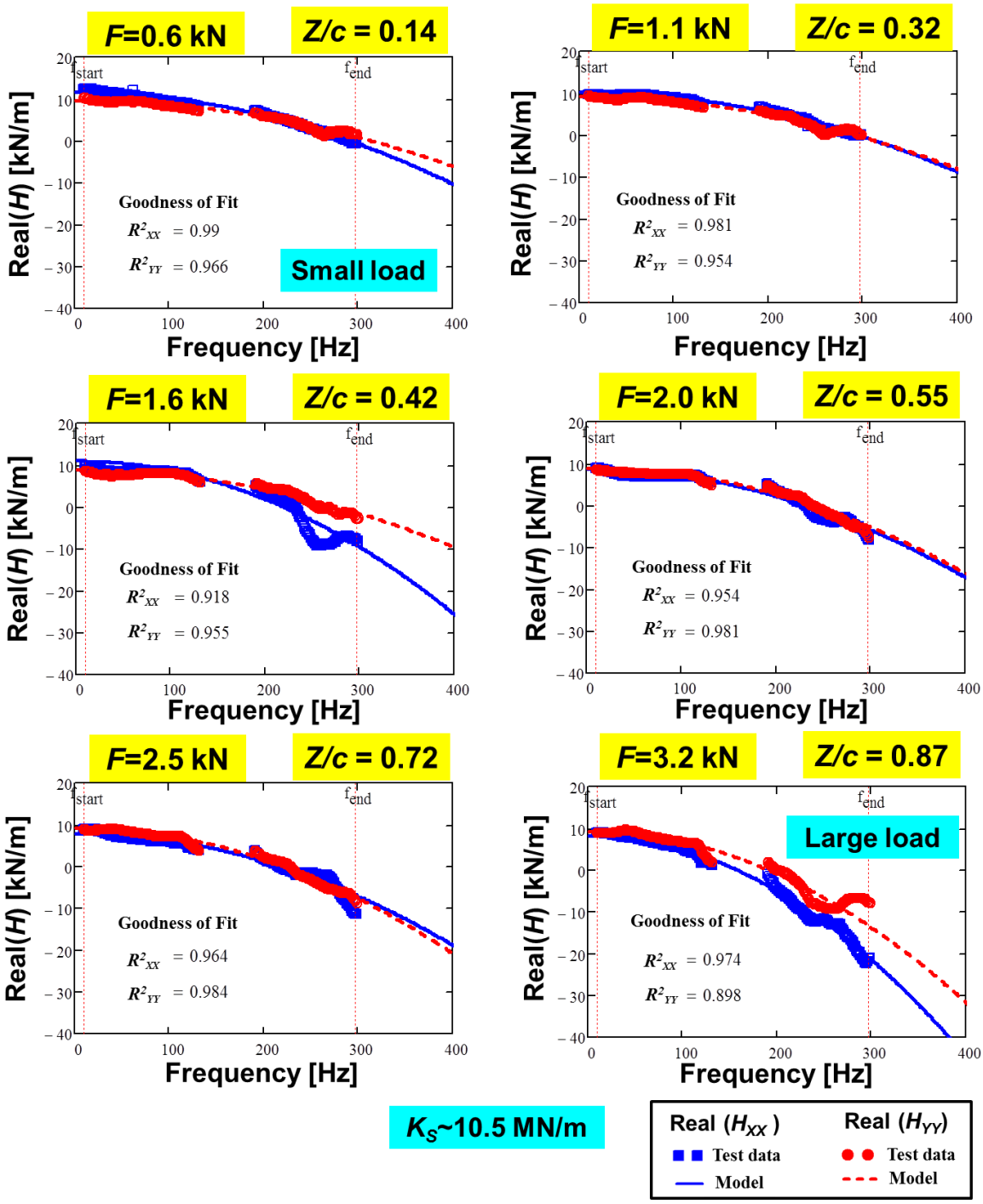

Figure 7. Real part of the test system direct impedances (H_{XX}, H_{YY}) versus excitation frequency. Tests with impact loads (0.5 – 3.2 kN) with amplitudes Z/c=0.14 - 0.87. Centered condition (e_S=0.0c). Test data and model fits. Open-ends SFD with c=213 μm and film land L=25.4 mm. Average of 10 impacts.

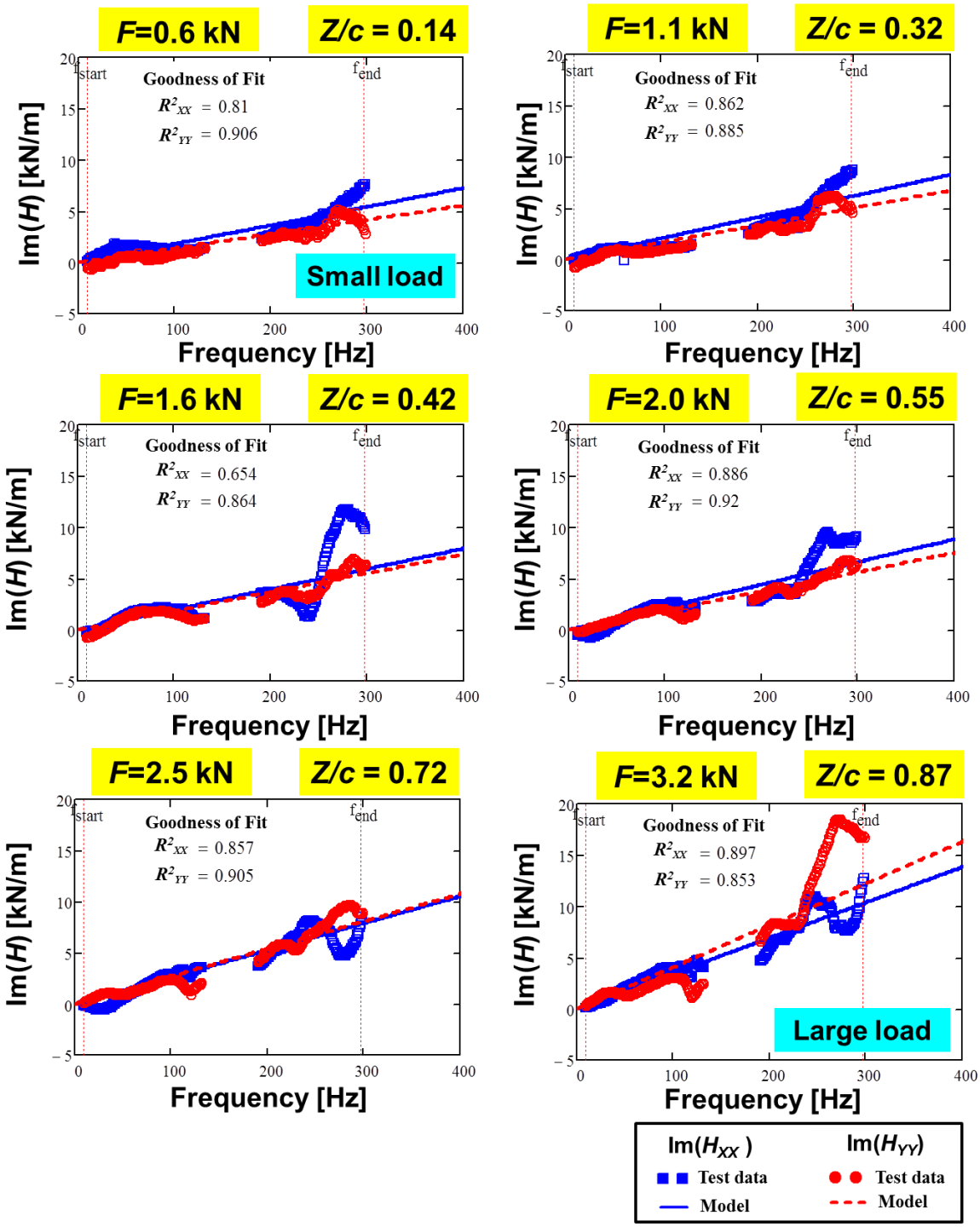

Figure 8. Imaginary part of the test system direct impedances (H_{XX}, H_{YY}) versus excitation frequency. Tests with impact loads (0.5 – 3.2 kN) with amplitudes Z/c=0.14 - 0.87 and centered condition (e_S=0.0c). Test data and model fits. Open-ends SFD with c=213 μm and film land L=25.4 mm. Average of 10 impacts.

Figures 9 through 11 depict the identified SFD[7] direct and cross-coupled force coefficients (damping, inertia and stiffness) obtained from the increasing impact load tests (0.5 - 3.2 kN) and ensuing BC amplitudes (Z) and at the centered condition (e_s = 0.0c).

The SFD cross-coupled damping coefficients (C_{XY}, C_{YX}) are at least an order of magnitude lower than the direct damping coefficients (C_{XX}, C_{YY}) and are nearly invariant to the size of the BC displacement.

The SFD direct damping coefficients (C_{XX}, C_{YY}) in Figure 9 increase moderately with increasing BC displacement up to $Z/c \leq 0.55$, and then grow more rapidly for larger Z/c. Overall, the identified SFD C_{XX} and C_{YY} are more or less similar up to $Z/c \leq 0.55$; however, they differ by as much as 16% at Z/c=0.87. In other words, the experimental SFD dynamic force coefficients (C_{XX}, C_{YY}) tend to diverge from each other as the BC amplitudes increase indicating that the magnitude of damping generated from SFD depends on its direction. Moreover, the difference in magnitude of C_{XX} and C_{YY} at small amplitude motions, Z/c=0.1,4 indicates the journal on one direction may have a smaller or larger radial clearance than the other (manufacturing tolerance).

The added mass coefficients (M_{XX}, M_{YY}) shown in Figure 10 increase with an increasing BC peak amplitude (Z). Recall that the slope of Re(H) curve grows increasingly negative as the amplitude of the BC displacement increases (see Figure 7). At Z/c=0.93, the fluid film added mass coefficient is ~6 kg, which is ~39% of the mass of the BC (15.15 kg). The SFD cross-coupled added masses are an order of magnitude lesser than M_{XX} and M_{YY} and insensitive to the BC excited displacement amplitude.

The SFD direct stiffness coefficients (K_{XX}, K_{YY}) shown in Figure 11 are less than 30% of structural stiffness (K_S =10.9 MN/m) whereas the cross-coupled stiffness coefficients (K_{XY}, K_{YX}) are more or less zero, K_{XY}, $K_{YX} \approx 0$, for all test conditions.

Appendix E presents the procedure for calculation of uncertainty in the force coefficients. In general, the total uncertainty for the identified direct damping (C), added mass (M), and stiffness (K) are U_C <8.1%, U_M <14.7%, and U_K <3.8% of the measured value, respectively. Note the force coefficients and uncertainties are valid exclusively over the noted identification frequency range (10-300 Hz).

[7] These are NOT truly linearized coefficient as the amplitudes are very large.

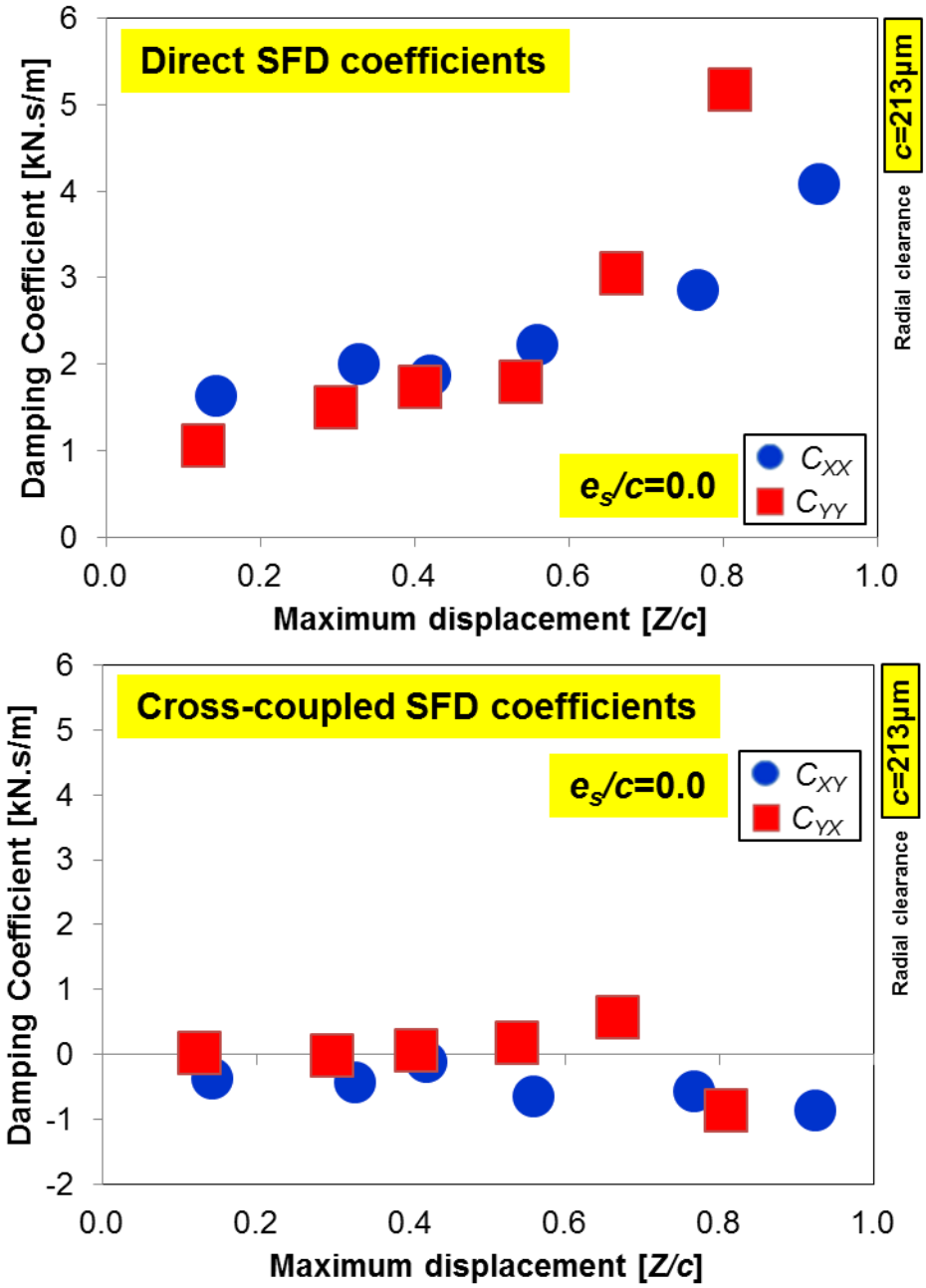

Figure 9. SFD direct and cross-coupled damping (C_{XX}, C_{YY}, C_{XY}, C_{YX}) coefficients versus peak BC displacements. Open-ends SFD with c=213 µm and 25.4 mm length film land. Parameters identified at centered condition e_S/c=0.0. Average of 10 impact loads.

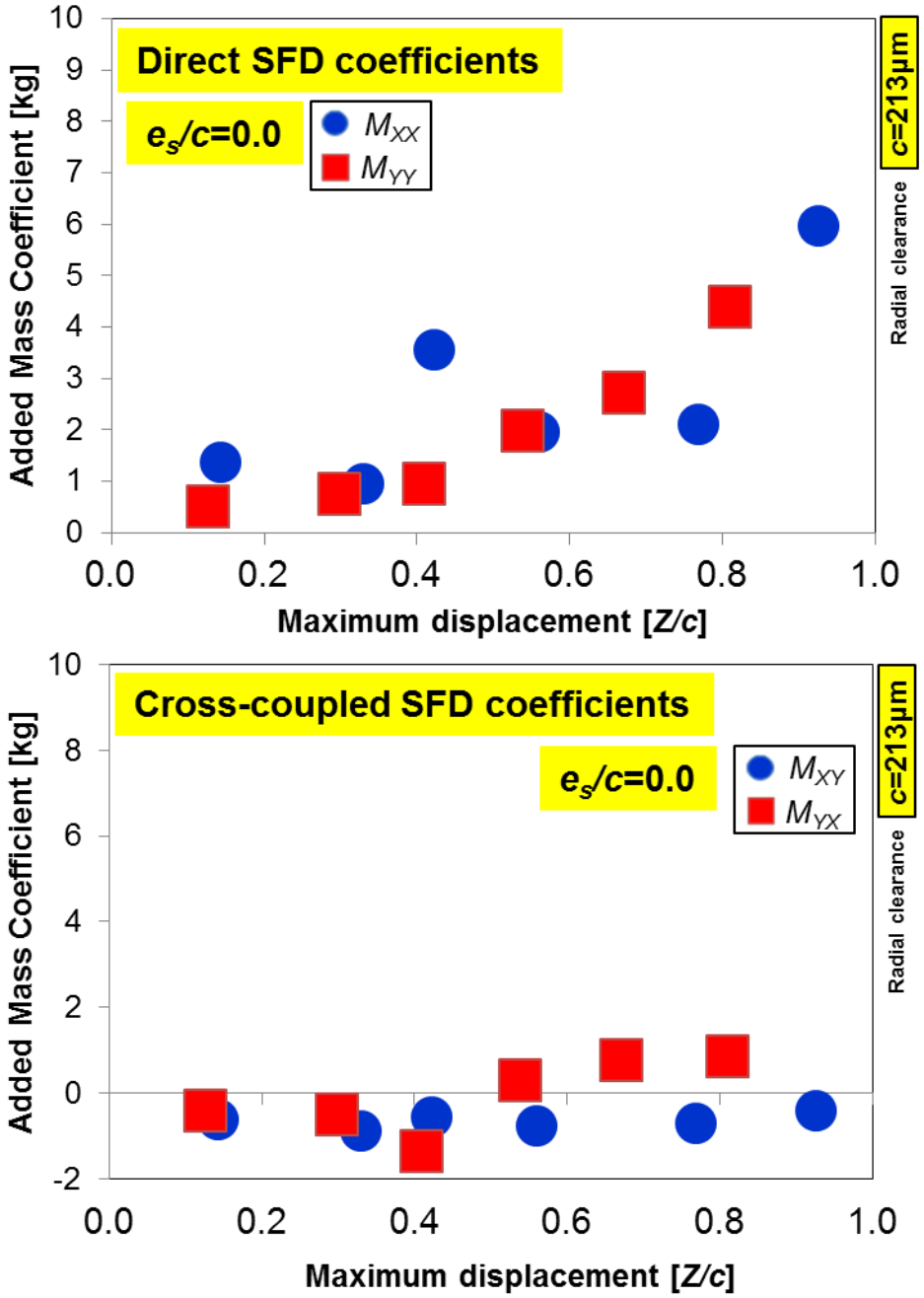

Figure 10. SFD direct and cross-coupled added mass (M_{XX}, M_{YY}, M_{XY}, M_{YX}) coefficients versus peak BC displacements. Open-ends SFD with c=213 µm and 25.4 mm length film land. Parameters identified at centered condition e_S/c=0.0. Average of 10 impacts.

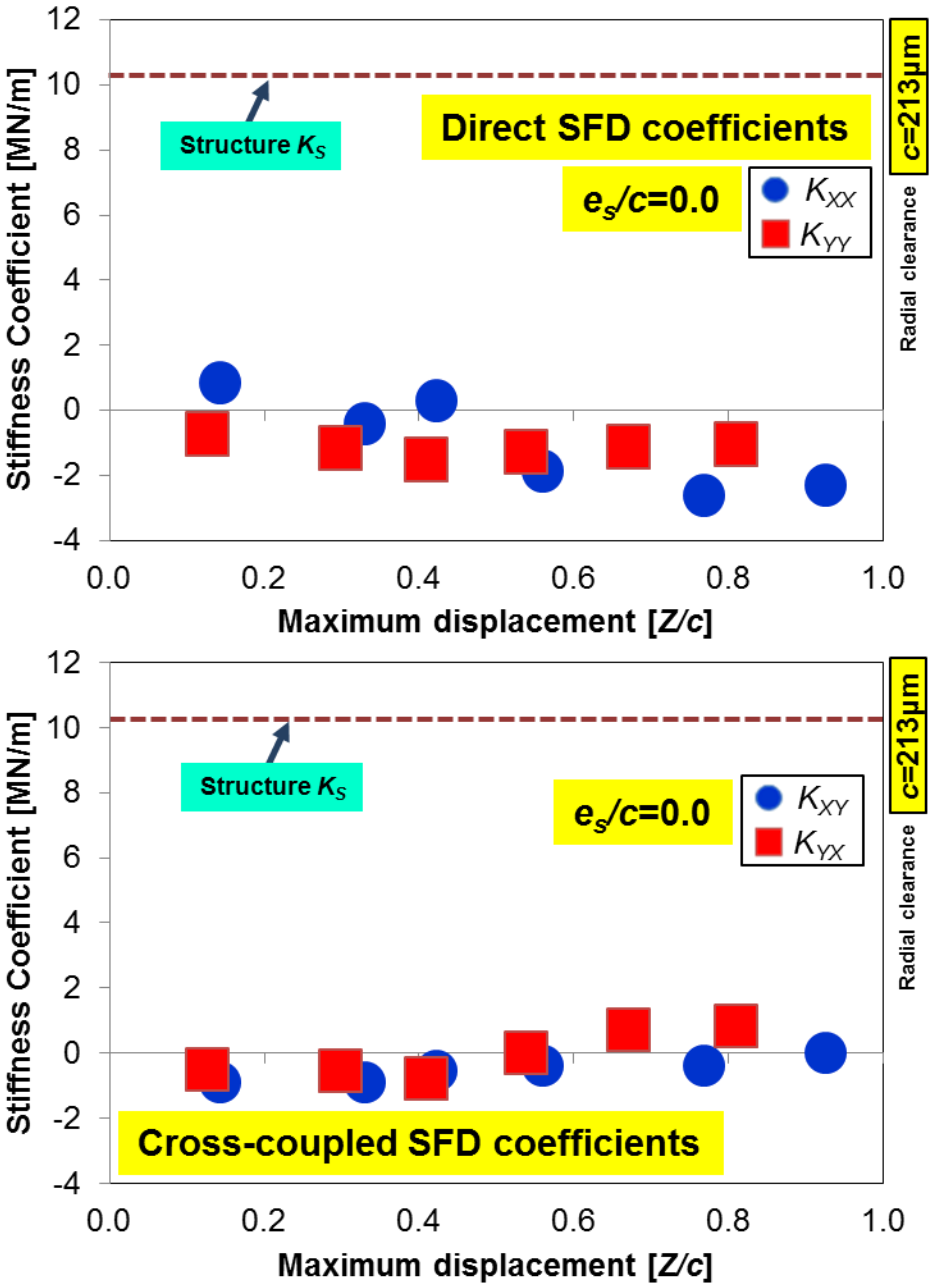

Figure 11. SFD direct and cross-coupled stiffness (K_{XX}, K_{YY}, K_{XY}, K_{YX}) coefficients versus peak BC displacements. Open-ends SFD with c=213 µm and 25.4 mm length film land. Parameters identified at centered condition e_S/c=0.0. Average of 10 impacts.

Effect of SFD force coefficients on damping ratio and logarithmic decrement

The damping factor (damping ratio) ζ and logarithmic decrement (log dec) δ are common ways to describe the level of damping in a system. Moreover, the experimental SFD force coefficients $(\mathbf{K}, \mathbf{C}, \mathbf{M})_{SFD}$ can be characterized in terms of both the damping ratio(ζ) and log dec (δ).

For example, the response of an underdamped (ζ) one degree of freedom system about its equilibrium position can be written as

$$X(t) = e^{-\xi\omega_n t}(A\cos\omega_d t + B\sin\omega_d t) \tag{5}$$

where

$$\zeta = \frac{C_L}{2\sqrt{K_L M_{tot}}},\ \omega_n = \sqrt{\frac{K_L}{M_{tot}}},\ \omega_d = \omega_n\sqrt{1-\xi^2} \tag{6}$$

and where A and B are real constants, ω_n is the natural frequency. M_{tot} includes the M_L and mass of the BC (M_{BC}). The log dec (δ) is the natural log of the ratio of the amplitudes of any two successive peaks separated by nth number of peaks.

$$\delta = \frac{1}{n}\ln\left(\frac{X_k}{X_{k+n}}\right) = \xi\omega_n\tau_d = \frac{2\pi\xi}{\sqrt{1-\xi^2}} \tag{7}$$

where $\tau_d = {2\pi}/{\omega_d}$ is the damped period of motion. Note that the log dec also can be determined directly from a measured transient motion response by calculating the ratio of a peak to the nth ensuing peak. The use of Eq. (7) in conjunction with experimental data is a convenient method for determining a system damping characteristics.

Figure 12 shows the exponentially decaying displacement transient response overlaid with the damping envelope for test data with peak displacements Z_X/c=0.14, 0.42, and 0.87. For a better comparison of all the presented test conditions, the BC displacements are normalized with respect to the BC maximum peak amplitude such that, $\overline{Z} = {Z}/{Z_{Max-peak}}$. Hence, the maximum dimensionless displacement $\overline{Z}$ is equal to one. The damping envelope curve ($e^{-\xi\omega_n t}$) represents the damping factor which is estimated from the identified SFD force coefficients. The BC amplitude decreases within the envelope of decaying exponential.

Figure 13 depicts the estimated system damping ratio (ζ) and log dec (δ) from the identified SFD force coefficients ($\mathbf{K}$, $\mathbf{C}$, $\mathbf{M}$)$_{SFD}$ versus increasing peak BC displacement (Z) from the centered condition (e_s=0). The results show that the log dec are approximately proportional (linear) to the peak BC motions. For large BC peak amplitudes, Z/c=0.87, the log dec is ~2.7 times larger than that for small BC motions, Z/c=0.14. Most importantly, notice that the SFD damping coefficients increase by a factor of ~5 from Z/c=0.14 to Z/c=0.87 (see Figure 9). This difference between the rate of increment of the log dec and damping coefficient is the result of the added mass coefficient that also increases with BC displacement (see Figure 10). In other words, the damping and inertia coefficients are non-linear depending on the amplitude of motions; however, damping ratio ζ do not increase as much.

In addition, cursory analysis of Eq. (6) reveals that the damping ratio (ζ) should not raise as much as the damping coefficient. For large BC peak motions Z/c>0.7, the increase in SFD added mass coefficients, up to ~6 kg make ζ raise remain small. The results show that identifying the added mass coefficient provides a reliable base of data to validate forced performance of SFD.

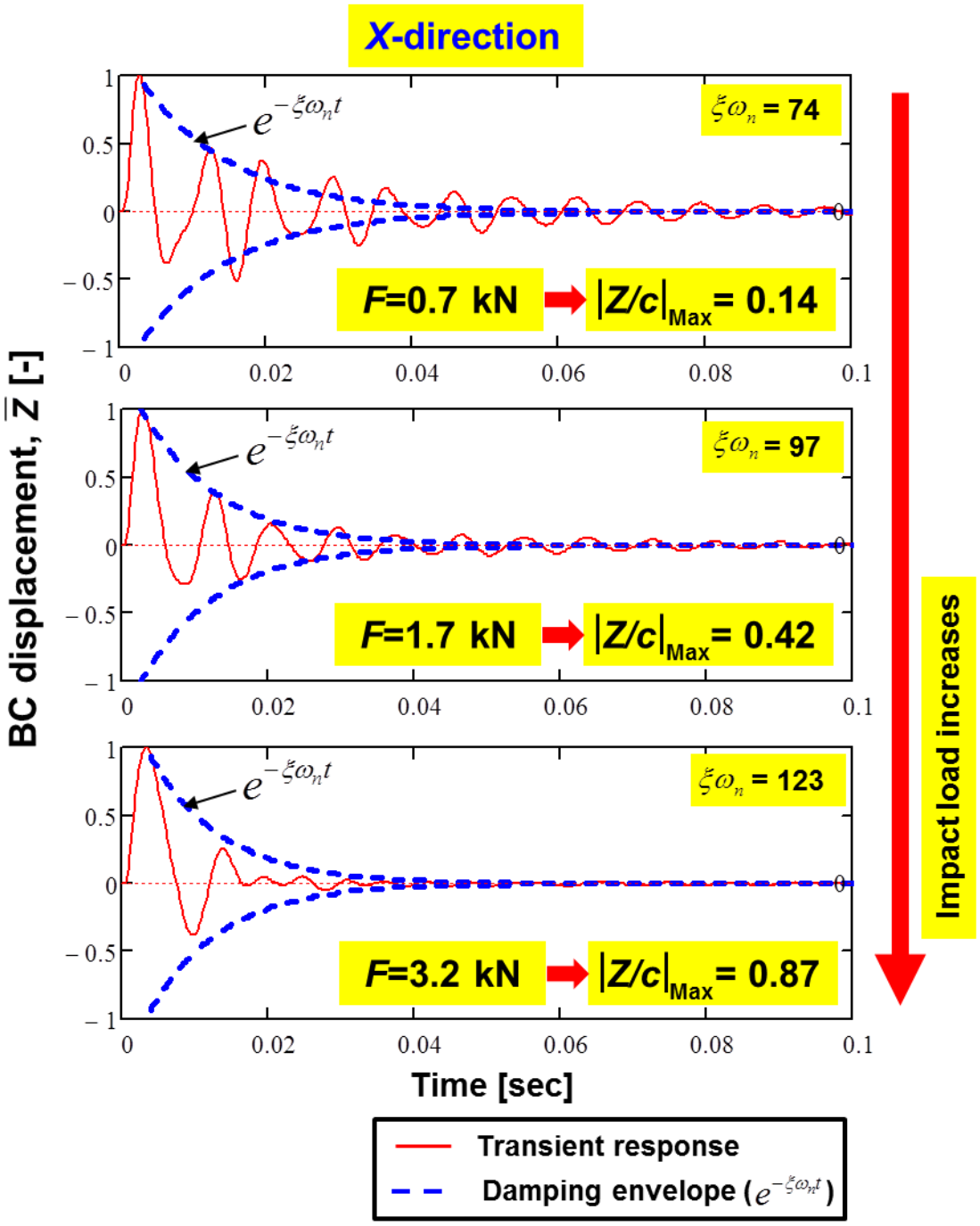

Figure 12. Dimensionless BC displacement ($\bar{Z}$) and damping envelope versus time (*t*). Measurements for Z_X/c=0.14, 0.42, and 0.87 at centered condition (e_s=0).

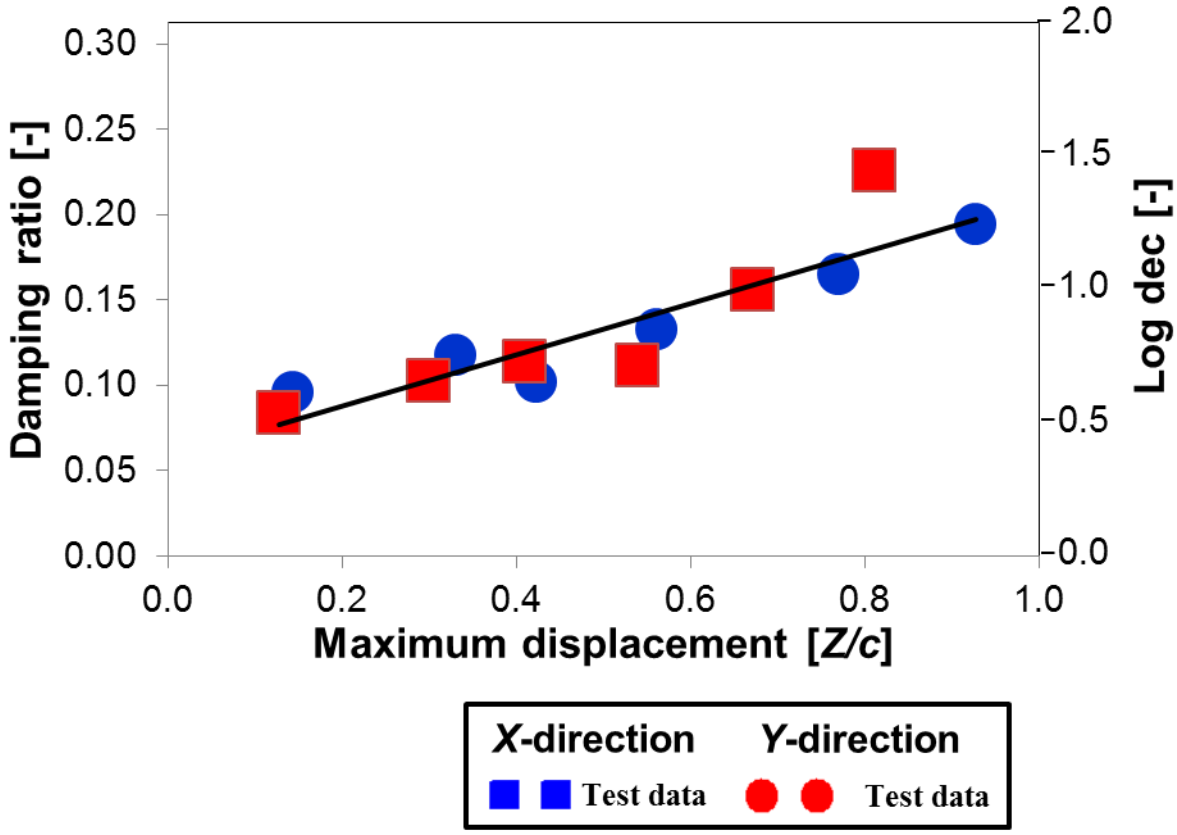

Figure 13. System damping ratio (ζ) and log dec (δ) versus peak displacement. Open-ends SFD with c=213 μm and 25.4 mm length film land. Parameters identified at centered condition e_S/c=0.0. Average of 10 impacts.

Recorded film pressures for test SFDs

This section presents an analysis of the film dynamic pressures as a function of the maximum BC displacement (Z) of the test damper.

Figure 14 shows the position of pressure sensors in the bearing cartridge (BC). Eight piezoelectric dynamic pressure sensors (P_1 – P_8) are installed in the BC around its circumference. Two sets of three pressure sensors ($P_{1\text{-}3}$ – $P_{4\text{-}6}$), spaced apart by 90º, record the dynamic pressure at the top, bottom and mid sections of the damper land as shown in the figure. Note that $P_{1\text{-}2\text{-}3}$ and $P_{4\text{-}5\text{-}6}$ are spaced 15º apart. Two other piezoelectric pressure sensors (P_7 and P_8) measure the film dynamic pressures at the exit of the squeeze film land.

Figure 15 depicts the *peak-to-peak* (*p-p*) dynamic film pressures versus the BC peak displacement (Z) for the open ends damper configuration (c=213μm). For impacts along the X-direction, the *p-p* pressures recorded at the top-half (z=+¼ L) and mid-plane (z=0), whereas the dynamic pressures for impacts along the Y-direction are measured at mid-plane (z=0) and bottom exit of the film land (z=-½ L). The data corresponds to increasing peak BC displacements (Z/c=0.13 - 0.93) at a centered condition (e_s=0). Increasing the impact load produces an increase in peak film pressures. The film pressures in the mid-plane (z=0) for both impact loads at X and Y directions are similar in magnitude. Notice that the pressure sensor P_4 (z=0) is located 120° away from applied load directions, X and Y (see Figure 15); hence the peak pressures at the film land along the load directions should be higher than the pressures recorded at P_4. The film pressures at the exit or bottom film land (z=-½L) in the journal are small, but they are ~3% of the peak pressures at the mid-plane.

Recall that for the open ends test damper (c=213μm), the lubricant supply pressure upstream of the feedholes was maintained at P_{in}~0.37 barg. The supplied oil flow rate, measured by a turbine flow meter, (Q_{in}) equals 4.5 LPM for the open ends damper.

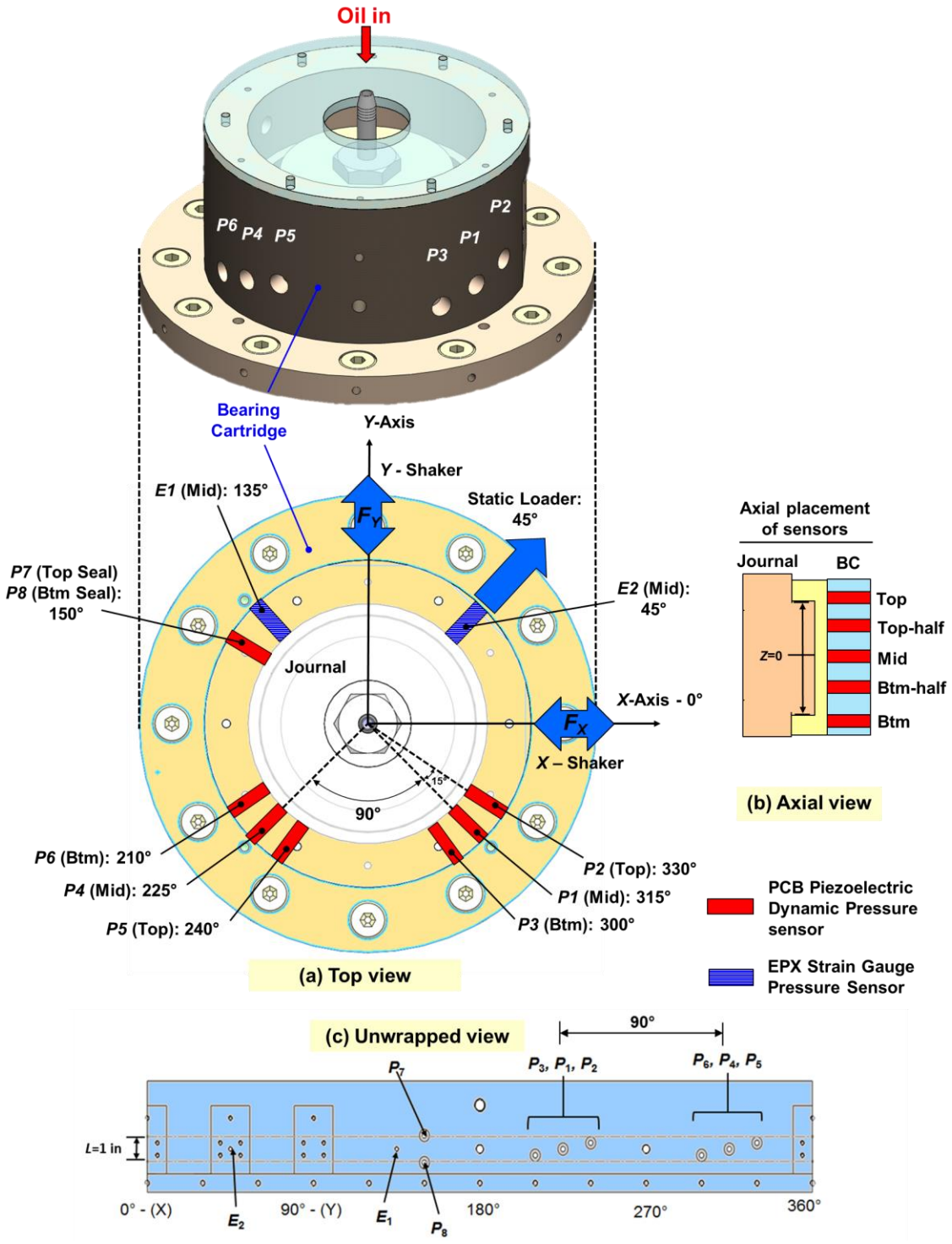

Figure 14. Schematic views of the disposition of pressure sensors in the BC: (a) top view, (b) axial view and (c) unwrapped view.

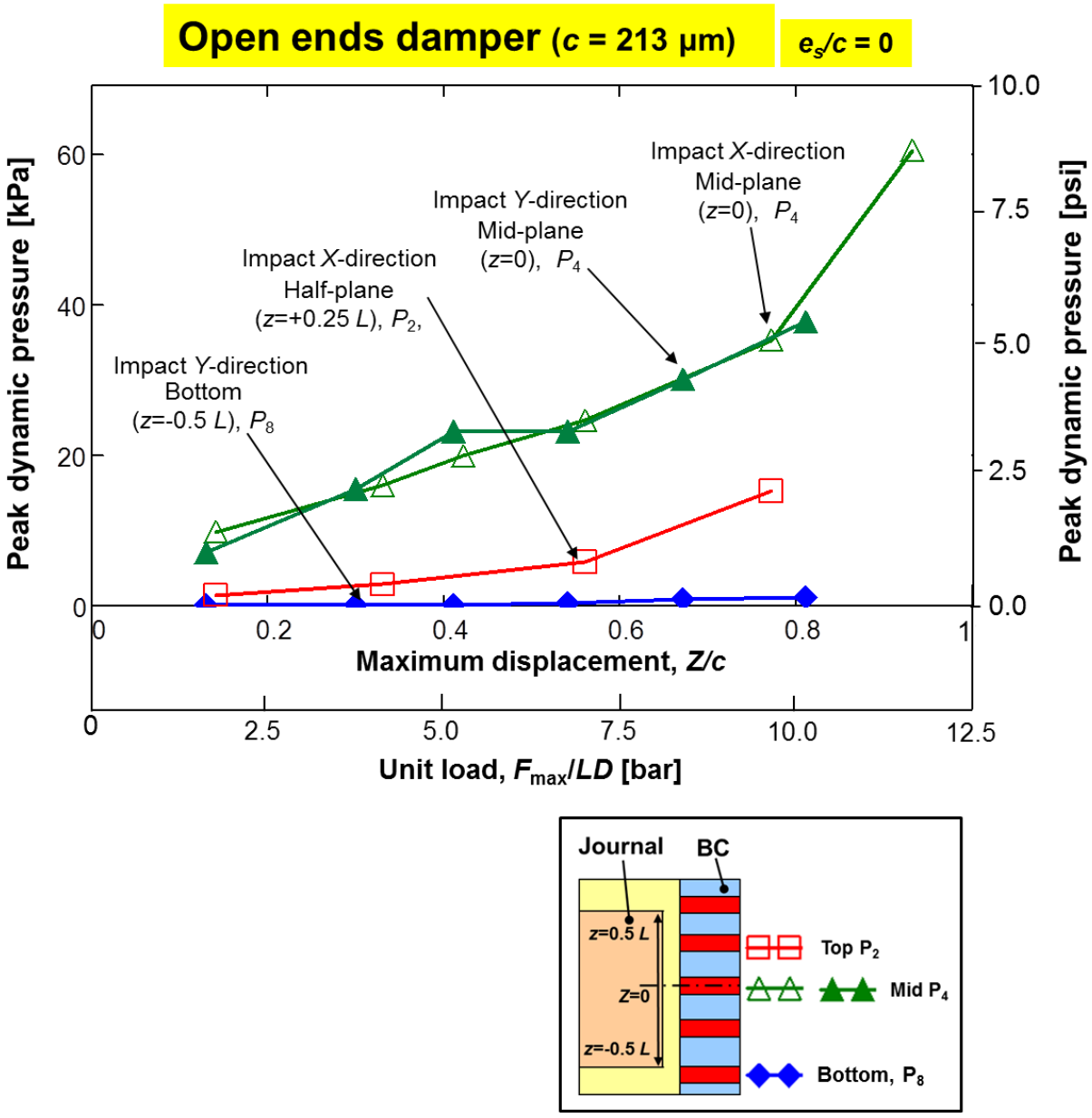

Figure 15. Recorded peak film dynamic pressures versus maximum BC displacement (*Z/c*). Open-ends SFD with *c*=213 μm and *L*=25.4 mm single film lands at centered condition e_S/c=0.0. Measurements at damper mid-plane, top (half-planes) and bottom exit. (Inset shows location of pressure sensors).

Figures 16 and 17 depict the time trace of dynamic pressures for sudden impact loads, 2.0 kN, along the X and Y directions, respectively. The dynamic pressures (P) are measured at the mid-plane (z=0, P_4), top-half (z=+¼ L, P_2), and bottom exit of the film land (z=-½ L, P_8). Notice the difference in vertical axis scales in Fig. 16 (a) and (b). The dynamic pressure profiles show an oscillatory response with an exponentially decaying amplitude that is similar to the responses of both the BC displacement and acceleration. All recorded dynamic pressures show peak at the instance of the sudden dynamic force on the BC. Note that P_4 is located 120° away from the applied load; thus showing a negative dynamic (suction) pressure due to an increasing (opening) of radial clearance at the instance of the impact.

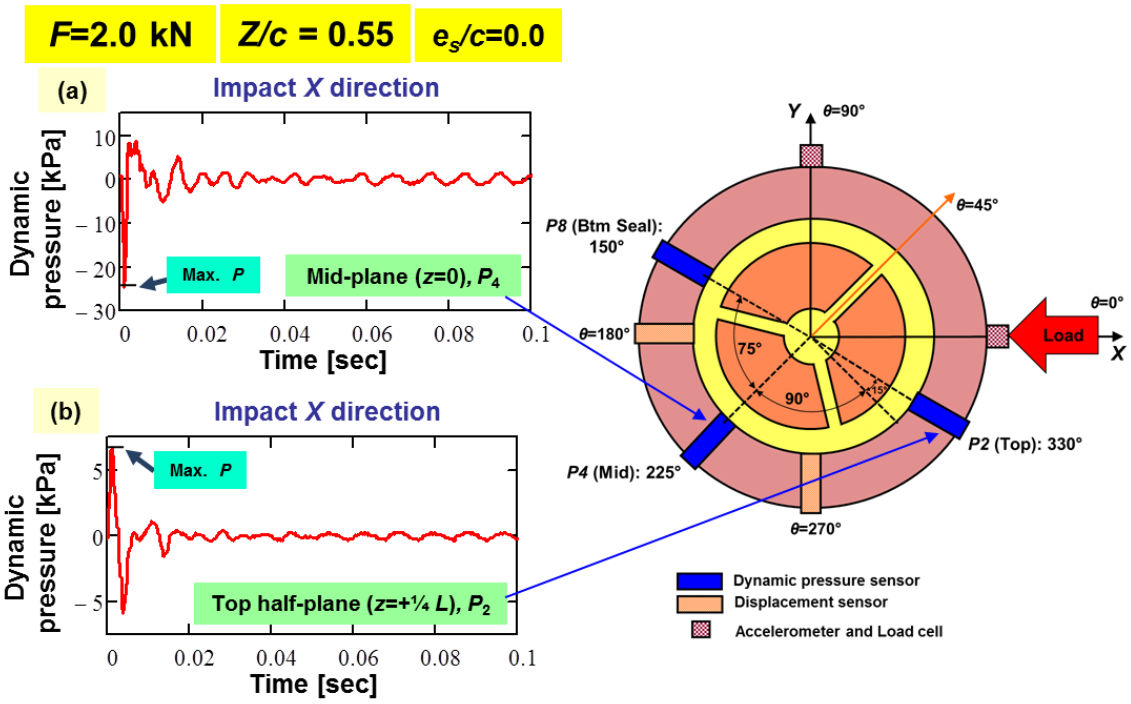

Figure 16. Dynamic film pressures (P) versus time (t) for measurements at mid-plane (z=0) and top half-plane (z=+¼L). Unidirectional load along X direction, F_X=2.0 kN, at journal centered condition (e_S/c=0). Graphs show data for orbits with magnitude Z/c=0.55. (nominal clearance c=213 μm, pressure supply at P_{in}~37 kPa).

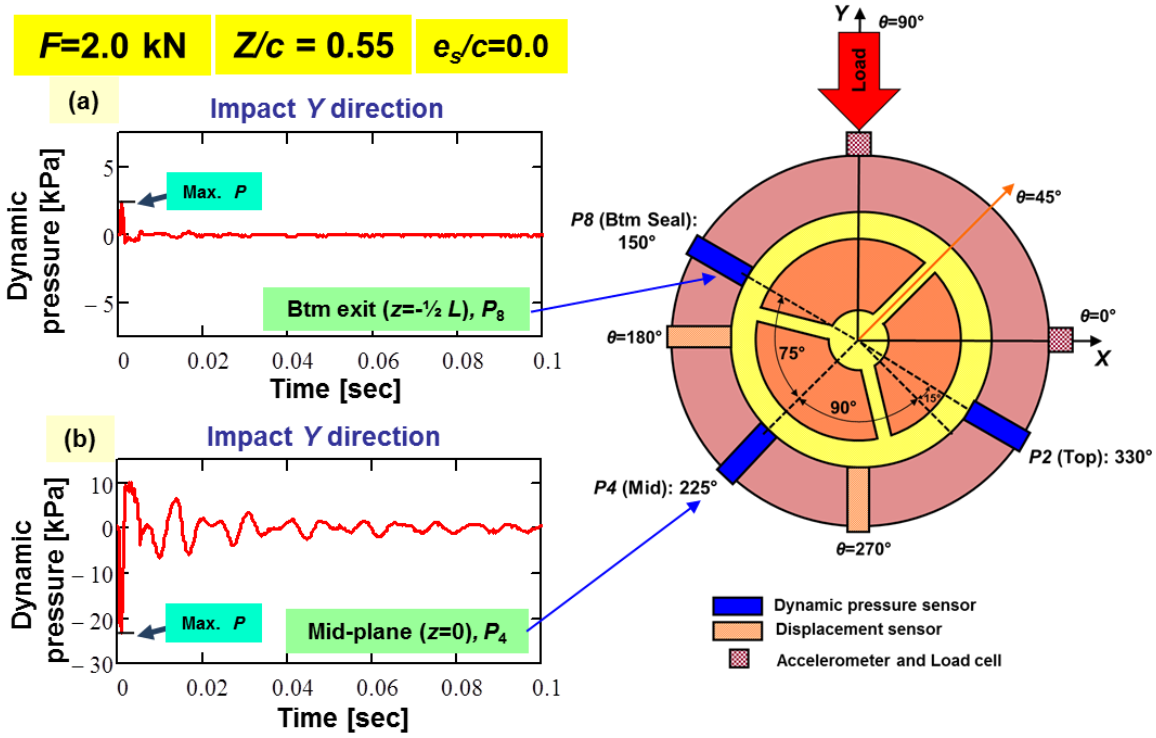

Figure 17. Dynamic film pressures (*P*) versus time (*t*) for measurements at mid-plane (*z*=0) and bottom exit of film land (z=-½*L*). Unidirectional load along *Y* direction, F_Y=2.0 kN, at journal centered condition (e_S/c=0). Graphs show data for orbits with magnitude *Z/c*=0.55. (nominal clearance *c*=213 μm, pressure supply at P_{in}~37 kPa).

Predicted versus experimental SFD force coefficients

This section provides a detailed comparison between the experimentally derived force coefficients and predicted force coefficients produced by an open ends SFD model. For reference, the short length, open ends SFD (2π-film, no oil cavitation) model predicts the direct damping and added mass coefficients [1] listed in Table 3. These coefficients refer to small amplitude motions about a centered equilibrium position e_s/c=0.

Table 3. Linearized force coefficients for open ends SFD [1]

Full film model (no cavitation)	
Direct damping coefficients	Direct added mass coefficients
$C_{XX} = C_{YY} = \frac{\mu D \pi}{2}\left(\frac{L}{c}\right)^3$	$M_{XX} = M_{YY} = \frac{\rho D \pi}{12}\left(\frac{L^3}{c}\right)$

where L=25.4mm. is the total film land length. Note that this model ignores the three feed holes and their orientation within the circumference of the bearing cartridge.

Figure 18 shows the experimental and predicted damping and added mass coefficients (recall the coefficients are identified over a frequency range 10 Hz – 300 Hz) versus peak BC displacement, Z/c=0.13 – 0.93. The direct damping coefficient predicted by the short length SFD model are within the uncertainty range (U_C <8.1%) of the experimentally identified C_{YY}. Albeit, the model under predicts C_{XX} by ~34% for a peak BC displacement of Z/c=0.14. The model either over predicts or under predicts the SFD direct added mass coefficient M_{XX} and M_{YY} by ~18% and ~53%, respectively, at a maximum displacement of Z/c=0.14.

The notable discrepancy between predictions (calculated with the formulas in Table 3) and test results of added mass coefficients can be attributed to not accounting for the three orifice feed holes that hold about ~40% of the lubricant volume in the film land for damper with c=213 μm (see **Appendix A**), for example.

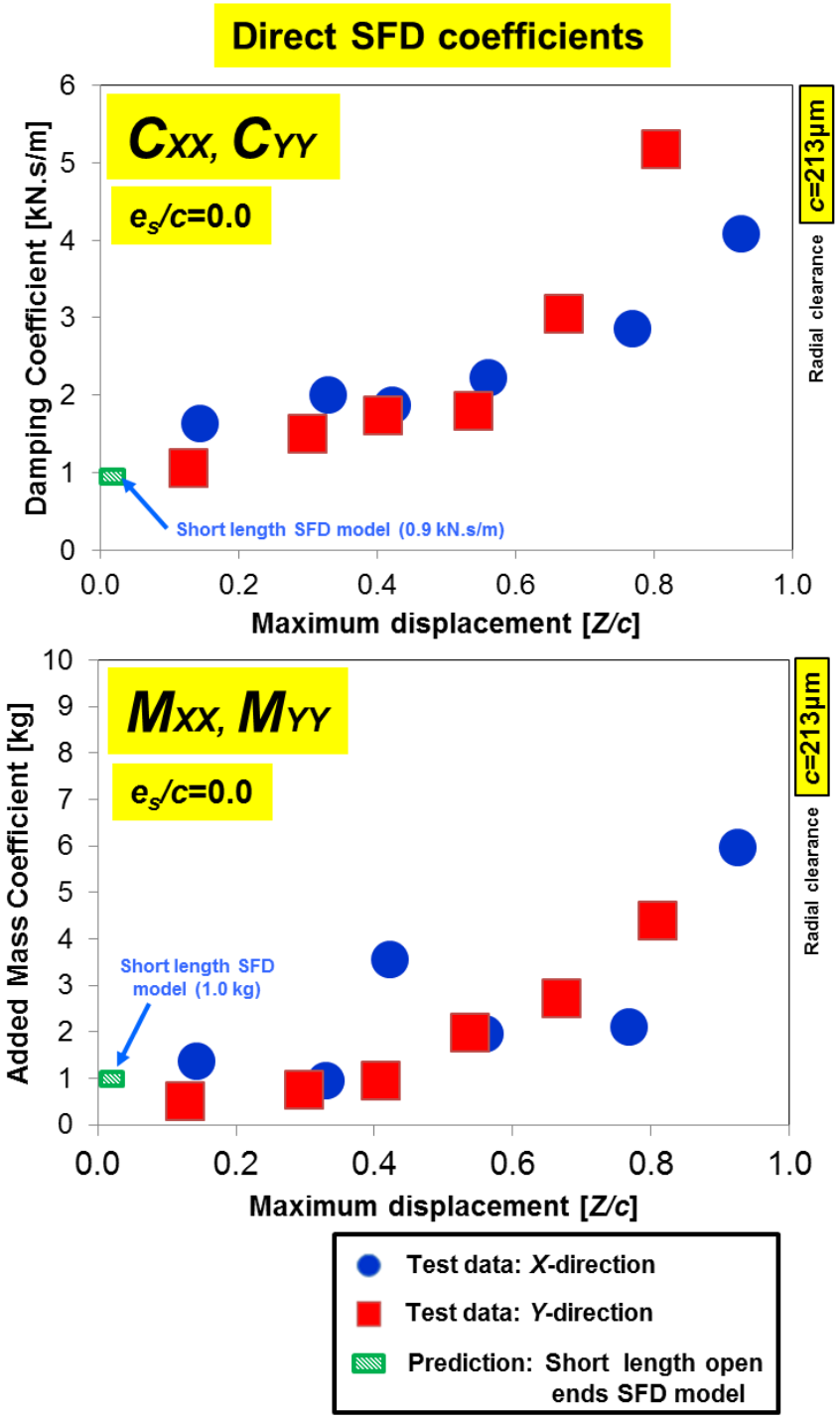

Figure 18. Experimental and predicted SFD direct damping coefficients (C_{XX}, C_{YY}) versus maximum BC displacement (Z/c) for circular centered (e_S/c=0) orbits. Open-ends SFD with c=213 µm and L=25.4 mm single film lands.

Conclusions and recommendations

This report interprets measurements and provides an analysis of force response obtained with a single land (L=25.4 mm) SFD from small to large amplitude impact loads, 0.5 - 3.2 kN and ensuing BC amplitudes, Z/c=0.14 – 0.87. The major conclusions derived from the measurements and predictions are:

Analysis of experimental force coefficients,

(a) SFD direct damping coefficients (C_{XX}, C_{YY}) increase with an increase in peak amplitude of unidirectional impact loads, but tend to grow rapidly about Z/c>0.55.

(b) SFD direct inertia coefficients increase almost linearly as the peak amplitude of BC motion increases.

(c) The SFD stiffness coefficients remain almost constant with an increase in peak BC amplitude (Z/c) and are less than 20% of structural stiffness (K_S).

(d) In general, SFD cross-coupled force coefficients (K, C, M) are minute in comparison to the direct force coefficients.

Damping ratios,

(a) Damping ratios increase approximately proportional to the peak BC motions. Increasing BC amplitude did not lead to a significant increase in damping ratios due to a large increase in added mass coefficients that suppress those rates of increment.

Film land dynamic pressures,

(a) An increase in BC amplitude leads to a proportional increase in *peak* dynamic film pressures.

Predictions and experimental results,

(a) Implementing classical formulas, the direct damping and added mass coefficients predicted by the short length, open ends SFD model agree modestly well within the uncertainty range of experimentally identified force coefficients. However, the model underestimates C_{XX} and either over predicts or under predicts the M_{XX} and M_{YY}, respectively. This discrepancy is due to the model not accounting for the three orifice feed holes.

Future work will include tests with intermittent impact excitations in order to better simulate actual operating conditions in multi-spool engines. The identification method will be extended to obtain the force coefficients obtained from intermittent impact loads with multiple frequencies. Further testing will enhance understanding of SFD response in dynamic impact applications and provide necessary data for design purposes.

Acknowledgement

Support of Turbomachinery Research Consortium (TRC) on the squeeze film damper research program is gratefully acknowledged. Special thanks to undergraduate student Jerry Haripin for his support in conducting the measurements.

References

[1] San Andrés, L., 2012, "Squeeze Film Damper: Operation, Models and Technical Issues," Modern Lubrication Theory, Notes 13, Texas A&M University Digital Libraries, https://repository.tamu.edu/handle/1969.1/93197

[2] Vance, J., Zeidan, F., Murphy, B., 2010, *Machinery Vibration and Rotordynamics*, "Bearings and Their Effect on Rotordynamics", Chapter 5, John Wiley & Sons, Inc., New York, pp. 216-238.

[3] Lattime, S., Steinetz, B., 2002, "Turbine Engine Clearance Control Systems Current Practices and Future Directions," Proceedings 38th AIAA/ASME/SAE/ASEE Joint Propulsion Conference & Exhibit 7-10 July 2002, Indianapolis, Indiana

[4] Lourenco, N., Graca, M., Franco, L., and Silva, O., 2007, "Fatigue Failure of a Compressor Blade," Eng. Failure Anlysis, **15**, pp1150-1154

[5] San Andrés, L., and Jeung, S.-H., 2013, "On the Forced Performance of a Squeeze Film Damper Operating with Large Amplitude Orbital Motions: Measurements and Assessment of the Accuracy of the Linearized Force Coefficients Model," TRC report, TRC-SFD-01-2013, May.

[6] Bradley, G., 2013, "Performance of a Short Open-end Squeeze Film Damper with Feed Holes: Experimental Analysis of Dynamic Force Coefficients," M.S. Thesis, Texas A&M Univ., College Station, TX., USA.

[7] Fritzen, C. P., 1985, "Identification of Mass, Damping, and stiffness Matrices of Mechanical System," ASME J. Vib., Acoust., **108**, pp9-16

Appendix A. Description of test system and components

This section provides a description of the journal, the bearing cartridge (BC) and the test rig components. References [A1,A2] give a full description of the SFD test rig.

Journal Figure A.1 presents views of a journal. The journal has a central through hole that acts as a lubricant flow path. The three equally spaced (120°) horizontal orifices (ϕ = 2.57 mm) distribute the oil to the squeeze film land at the mid-plane.

Figure A.2 shows a photograph of one orifice insert in the journal. The insert consists of a hex socket screw with an orifice hole of diameter 2.57 mm. The orifice design enables the number of active lubricant feedholes to vary by replacing the orifice insert with closed hex socket screw. A small hex screw holds ~0.29 mL volume of lubricant. Hence, the three orifices hold about ~40% of the lubricant volume in the film land (πDLc=2.57 mL) for damper with c=213 μm.

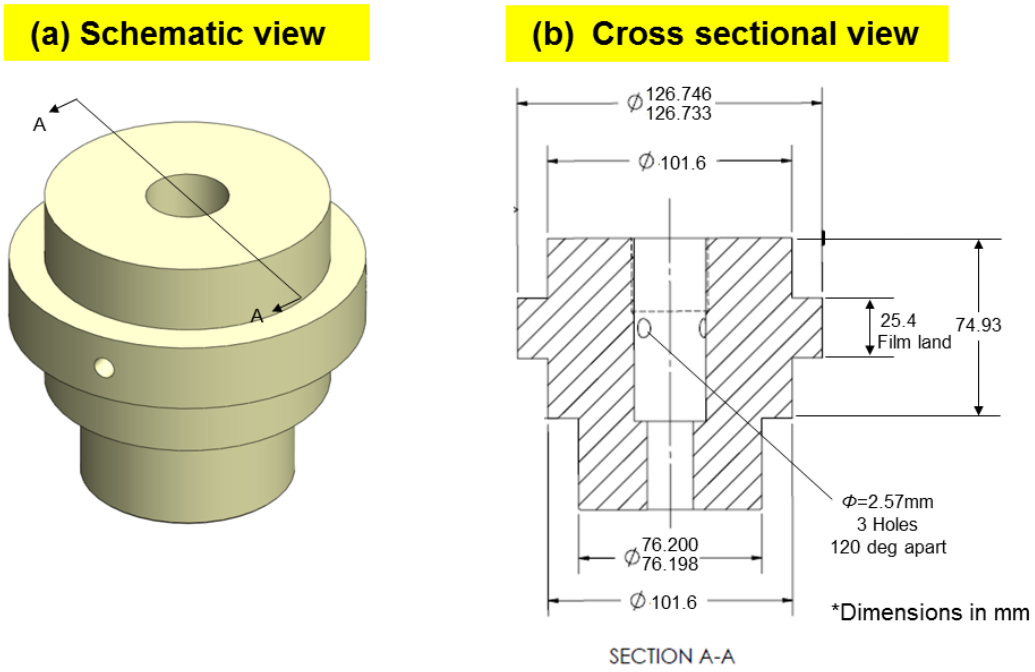

Figure A.1. Test journal (a) isometric view, and (b) cross sectional view. Squeeze film land length: 25.4 mm (Material: AISI 1018 carbon steel)

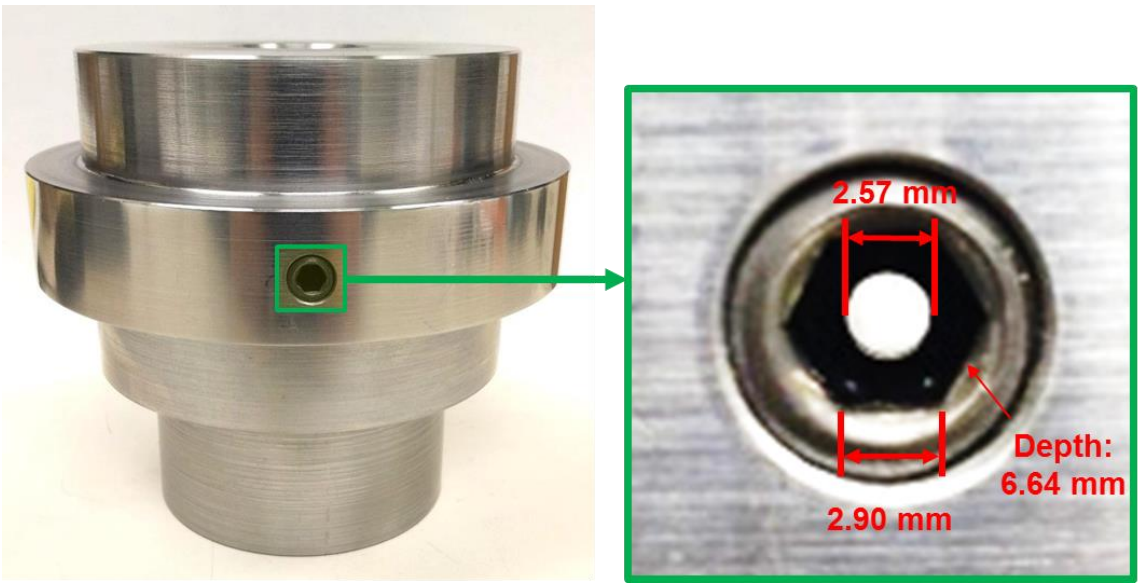

Figure A.2. Photograph of feed orifice design with small hex socket

Bearing Cartridge Figure A.3 depicts views of the bearing cartridge (BC). The BC does not have a central groove and the inner surface of the BC creates the outer surface of the squeeze film land with uniform thickness axially. The BC interfaces with four support rods and accommodates instrumentation including REBAM® sensors, load cells, accelerometers and pressure sensors.

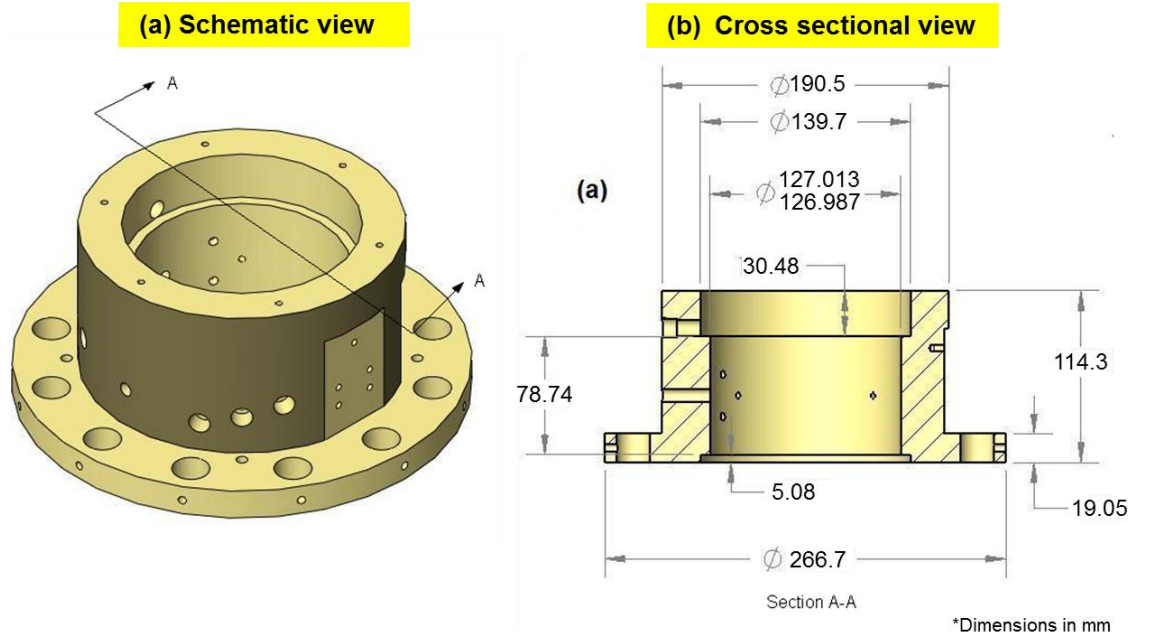

Figure A.3. Bearing cartridge (a) isometric view, and (b) cross sectional view. (Material: AISI 1018 carbon steel)

Measurement of journal outer diameter The radial clearance of the squeeze film damper is a critical design value. Half of the difference between the journal outer diameter and the BC inner diameter is the nominal clearance. A micrometer (uncertainty ±2.54 μm (0.1 mil) measures the specified axial planes and angles of the journal and BC as shown in the Figure A.4. Table A.1 lists the measured outer diameter of the journal at each plane and measurements of the BC inner diameter. The average SFD radial clearance is

$$c = \tfrac{1}{2}(D_{BC\_ID} - D_{J\_OD}) = 213.4\ \mu m\ (8.4\ mil) +/-\ 10\ \mu m$$

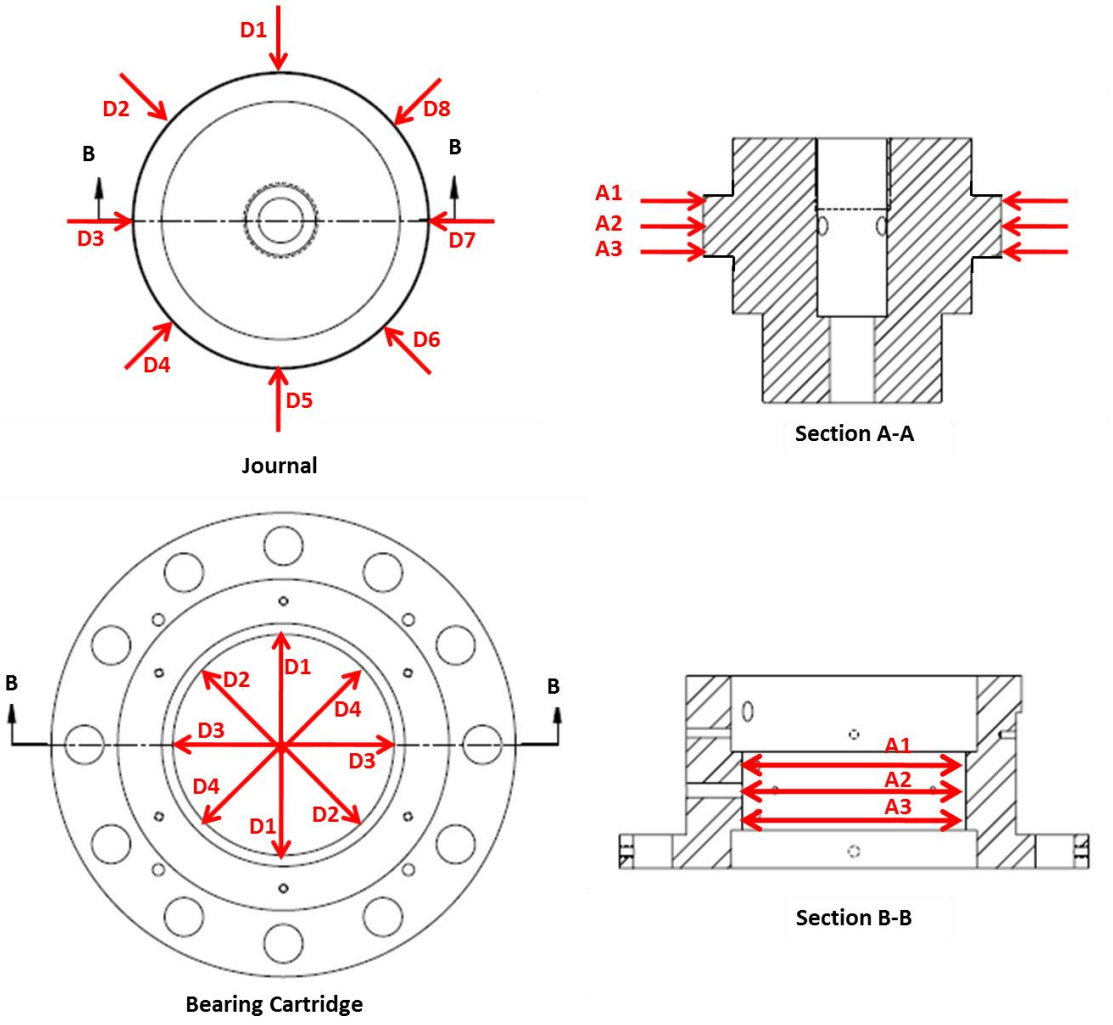

Figure A.4. Measurement planes for journal outer diameter and BC inner diameter (D planes are radial lines with constant spacing of 45º apart)

Table A.1. Measurements of journal outer diameter and BC inner diameter recorded at each plane described in Figure A.4 Estimated radial clearance.

Journal outer diameter

Measurement Plane	A-1 (Top) [cm]	A-2 (Mid) [cm]	A-3 (Btm) [cm]
D1 (X-axis)	12.6731	12.6774	12.6751
D2 (45-deg)	12.6728	12.6746	12.6736
D3 (Y-axis)	12.6738	12.6741	12.6754
D4 (135-deg)	12.6731	12.6741	12.6731
Total Grand Average:		12.6741	centimeters
Total Uncertainty: +/-		0.0003	centimeters

BC inner diameter

Measurement Plane	A-1 (Top) [cm]	A-2 (Mid) [cm]	A-3 (Btm) [cm]
D1 (X-axis)	12.7170	12.7168	12.7163
D2 (45-deg)	12.7168	12.7165	12.7163
D3 (Y-axis)	12.7165	12.7160	12.7160
D4 (135-deg)	12.7165	12.7165	12.7163
Total Grand Average:		12.7165	centimeters
Total Uncertainty: +/-		0.0003	centimeters

Measurement Plane	**Radial Clearance** [cm]
D1 (X-axis)	0.0208
D2 (45-deg)	0.0216
D3 (Y-axis)	0.0213
D4 (135-deg)	0.0218
Total Grand Average:	0.0213

References

[A.1] Jeung, S.-H., 2013, "Performance of an Open Ends Squeeze Film Damper Operating with Large Amplitude Orbital Motions: Experimental Analysis and Assessment of the Accuracy of the Linearized Force Coefficients Model," M.S. Thesis, Texas A&M Univ., College Station, TX., USA.

[A.2] Bradley, G., 2013, "Performance of a Short Open-end Squeeze Film Damper with Feed Holes: Experimental Analysis of Dynamic Force Coefficients," M.S. Thesis, Texas A&M Univ., College Station, TX., USA.

Appendix B. Measurement of lubricant properties and flow rate

The PW SFD test rig uses ISO VG 2 grade oil as its lubricant. A Brookfield DV-E rotary viscometer gives the viscosity of a lubricant by measuring the shear (drag) stress on a cylindrical spindle fully submerged in a lubricant bath. The viscosity of the ISO VG 2 lubricant was measured at increasing temperatures where a water jacket covering the lubricant heated the oil to various temperatures. The ASTM standard viscosity-temperature relation is

$$\mu = \mu_R e^{-\alpha_v (T - T_R)} \tag{B.1}$$

where μ_R = 2.60 cPoise (0.377 micro-Reyn) is the measured viscosity at room temperature (T_R = 23ºC). The oil viscosity coefficient, α_v, is given as

$$\alpha_v = \frac{-\ln(\mu_2 / \mu_R)}{(T_2 - T_R)} = 0.016 \frac{1}{^\circ C} \tag{B.2}$$

where μ_2 and T_2 are the last viscosity and temperature measurements, respectively.

Figure B.1 shows the measurements of lubricant viscosity along with a ASTM standard curve fit. The ASTM standard viscosity-temperature relation for the current measurements shows high correlation (R^2=0.998).

The measurements give 2.4 cSt (1.92 cPoise) at 40°C whereas the lubricant manufacturer specifies 2.1 cSt (1.68 cPoise) at the same temperature (see Table B.1). The difference, amounting to ~14%, is most likely due to entrapped air in the lubricant from numerous tests performed using the identical oil tank during the past research programs. Note that a 10% of entrained air (volume) can increases viscosity by up to 15% [B.1]. In addition, the blend of multiple batches of the same lubricant brand purchased at various times could also explain the difference in viscosity.

At ambient condition of 23°C, the lubricant density was also determined, by weighing a known volume of lubricant oil. The oil density obtained is ρ=800 kg/m^3.

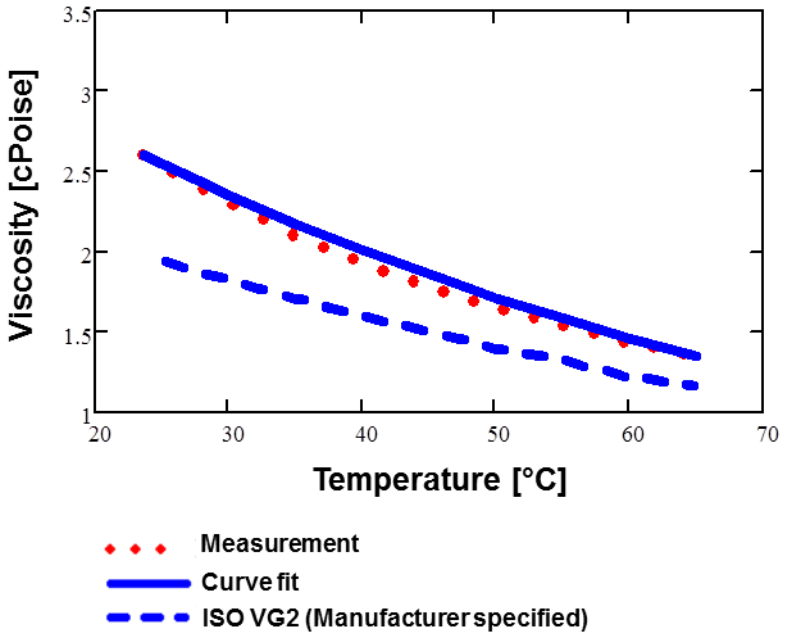

Figure B.1 Measured lubricant viscosity versus temperature. Viscosity measured with a rotary viscometer.

Table B.1 Mobil Velocite™ No 3 (ISO VG 2) Manufacturer specification [B.2]

Mobil Velocite Oil Numbered Series No 3 (ISO VG 2)	
cSt @ 40ºC	2.1
cSt @ 100ºC	0.95
Pour Point, ºC	-36
Flash Point, ºC	84
Density @ 15º C, kg/L	0.802

Figure B.2 shows a view of the lubricant flow path through the test damper with an accompanying simple hydraulic circuit. ISO VG 2 lubricant, supplied through the oil inlet with flow rate Q_{in} at inlet pressure P_{in}, flows through three orifices (ϕ=2.5 mm), 120º apart, each with hydraulic resistance R_o. The film land fills up with lubricant at feed hole pressure P_S and continuously discharges to the top and bottom lands with flow rates Q_T and Q_B, respectively. After the lubricant passes through the top and bottom film lands, each with a hydraulic resistances R_T and R_B, it exits to ambient, P_a=0 bar(g).

To measure flow rate through the test rig, ISO VG 2 grade lubricant is supplied at room temperature (23 ºC) to the journal at a centered condition (e_s=0). The inlet flow rate and at least one output flow rate (Q_T or Q_B) must be known. The oil delivery piping houses a turbine type flow meter to measure the inlet flow rate directly. Note that all air was evacuated from the oil lines prior to measurements. The outlet flow rate through the bottom land (Q_B) is determined by measuring the amount of time it takes to fill the oil collector to a known volume.

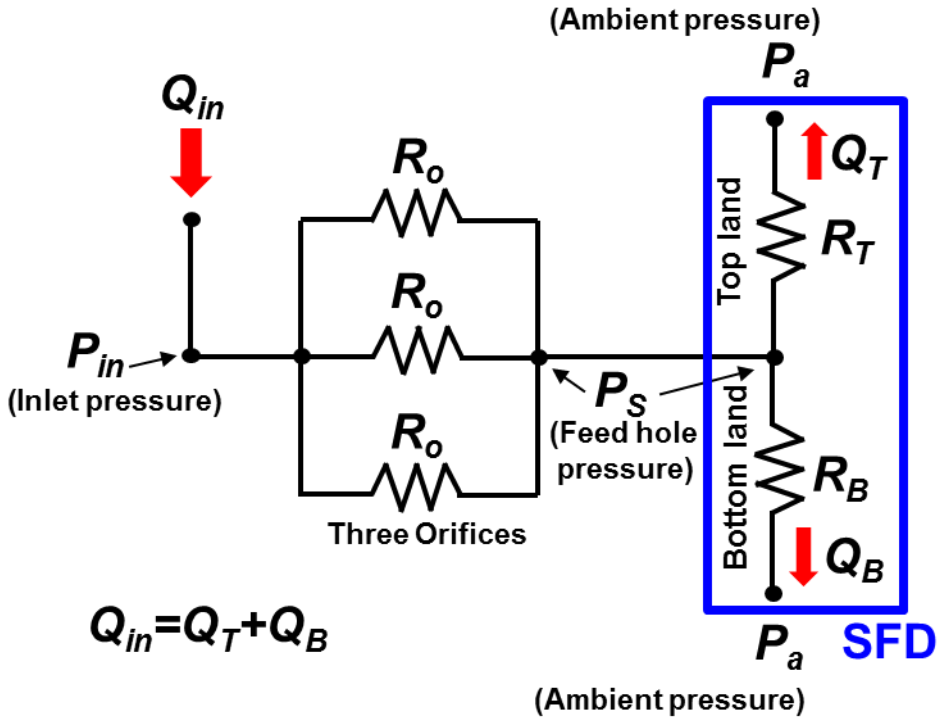

Figure B.2 Hydraulic circuit diagram for open ends SFD.

Table B.2 lists the recorded static pressure (P_{in}), flow rate, and ratio Q_B/Q_{in} for the damper configuration tested. In all tested pressures and flow rates, the bottom land flow rate Q_B is ~56% of the inlet flow rate Q_{in}. These measurements show that the lubricant is close to being evenly distributed to the top and bottom lands since nearly 44% of inlet flow must exit from the top land.

Table B.2. Measured inlet pressures and lubricant flow rates. ISO VG 2 oil at room temperature T_S=23°C

P_{in} (barg) [±0.003]	Q_{in} (LPM) [~5%]	Q_B (LPM) [~5%]	Ratio Q_B/Q_{in}
0.06	2.0	1.1	0.55
0.21	3.4	2.0	0.57
0.37	4.5	2.4	0.54
0.59	5.8	3.3	0.56
Average			0.56

References

[B.1] "Ten Things You Probably Didn't Know About Air Contamination", 2007, Industrial Lubricants, Machinery Lubrication, Accessed October 2013, http://www.machinerylubrication.com/Read/1088/air-contamination-oil

[B.2] "Mobil Velocite™ No 3 (ISO VG 2) Manufacturer specification sheet", Hydraulic oils Typical Properties, Mobil, Accessed October 2013, http://www.mobil.com/USA-English/Lubes/PDS/GLXXENINDMOMobil_Velocite_Oil_Numbered.aspx

Appendix C. Identification of (dry system) test structure parameters

Four main rods support the current bearing cartridge (BC). Figure C.1 displays a schematic view of the static load test setup. One eddy current REBAM® displacement sensor is mounted externally via a magnetic base and aligned with the *X*, *Y*, or 45^o direction. This sensor is referred to as an external sensor and has a known sensitivity. By measuring the force from the static loader, data from the external sensor can be used to measure the stiffness of the test rig.

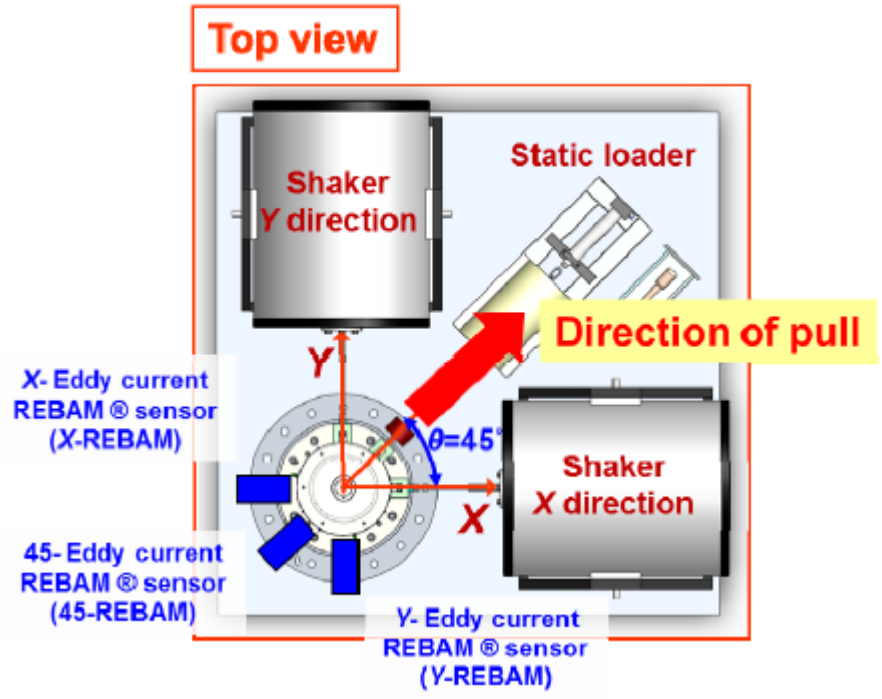

Figure C.1. Schematic view of static load test setup

Figure C.2 shows BC displacement versus the static load applied for each orientation of the external sensor. The estimated structural stiffness is K_S=10.9 MN/m for a BC displacement the direction of applied load. Along the *X* and *Y* axes, the stiffnesses are K_{SX}=10.6 MN/m and K_{SY}=11.1 MN/m, respectively. Note that the structural stiffness along the *X* axis is ~5% smaller than the that of *Y* axis.

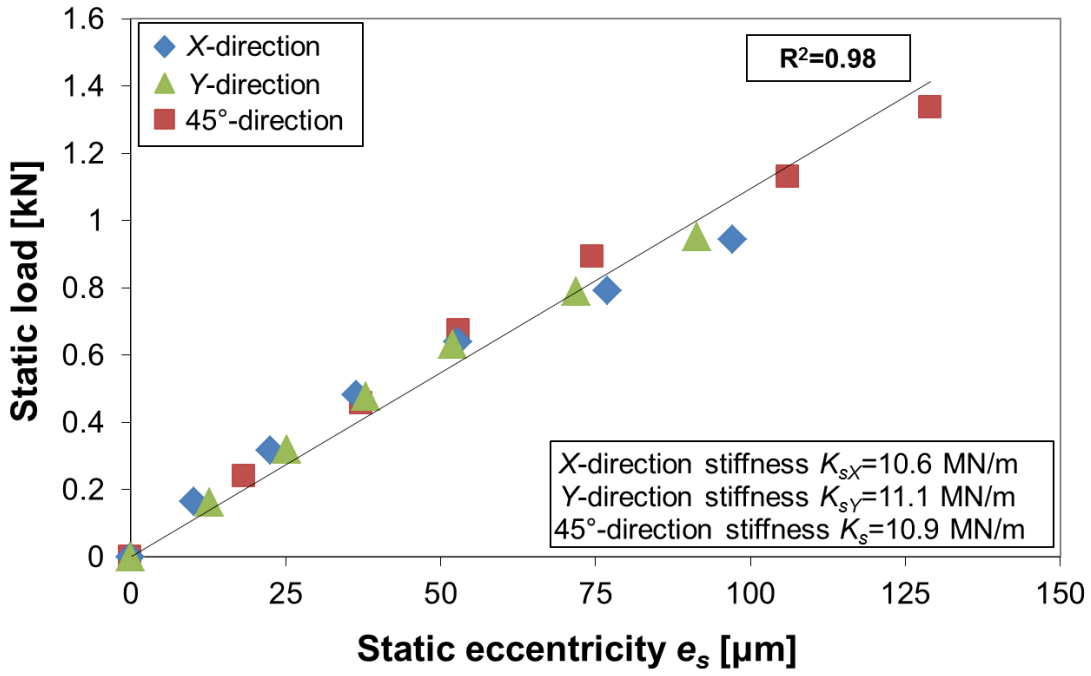

Figure C.2. Static load versus BC displacement and estimated structural stiffness along the *X*, *Y* axes and along the 45º direction.

The REBAM© displacement sensors show a reduction of its quoted sensitivity (~ 1 V/1mil) when installed in the BC wall and facing the target journal. The reduction is due to the metal surrounding the probe tip. Thus, the REBAM© sensors are calibrated in place for accurate measurements. The calibration was easily accomplished by comparing the digital readout of voltage between the displacement sensors mounted externally and installed in the BC when subjected to a static load. The sensitivities determined are 0.75 V/mil and 0.77 V/mil for the *X* and *Y*-axis sensors, respectively. These sensitivities are lower, as expected, than the manufacturer rating of 1 Volt/mil.

Table C.1 lists the identified test system structural parameters (K_s, C_s, M_s) over a excitation frequency range from f_{start}=10 to f_{end}=250 Hz. Recall that the structure (static load) stiffness is K_{SX}=10.6 MN/m and K_{SY}=11.1 MN/m along the *X* and *Y* directions. Dynamic load tests reveal K_{sXX}=10.1 MN/m and K_{sYY}=10.9 MN/m, approximately ~5% smaller than K_{SX} and K_{SY}.

Figure C.3 shows the experimental data and physical model fits in real and imaginary parts of *H*. The goodness of physical model fits shows $R^2 > 0.95$ for the real part of *H* implying the model represent well the test structural system. On the other hand, the

correlation for the imaginary part of H are relatively low indicating the structural damping (C_s) is not of viscous type.

Table C.1. System structural parameters obtained from circular orbit tests under a dry condition (no lubricant). Parameters identified in frequency range 100–120 Hz and 200-250 Hz. Orbit amplitude *r/c*=0.04 and static eccentricity e_s/c=0.0.

Frequency range 10 - 250 Hz						
Structural parameter			Direct		Cross-coupled	
			XX	*YY*	*XY*	*YX*
Stiffness	K_s	[MN/m]	10.1	10.9	0.31	-0.11
Damping	C_s	[kN.s/m]	1.1	0.9	0.51	0.70
Residual mass	M_s	[kg]	1.9	2.1	0.12	0.15
System Mass	M_{BC}	[kg]	15.15			
Natural frequency	f_n	[Hz]	130	135		
Damping ratio	ξ_s		0.04	0.04		

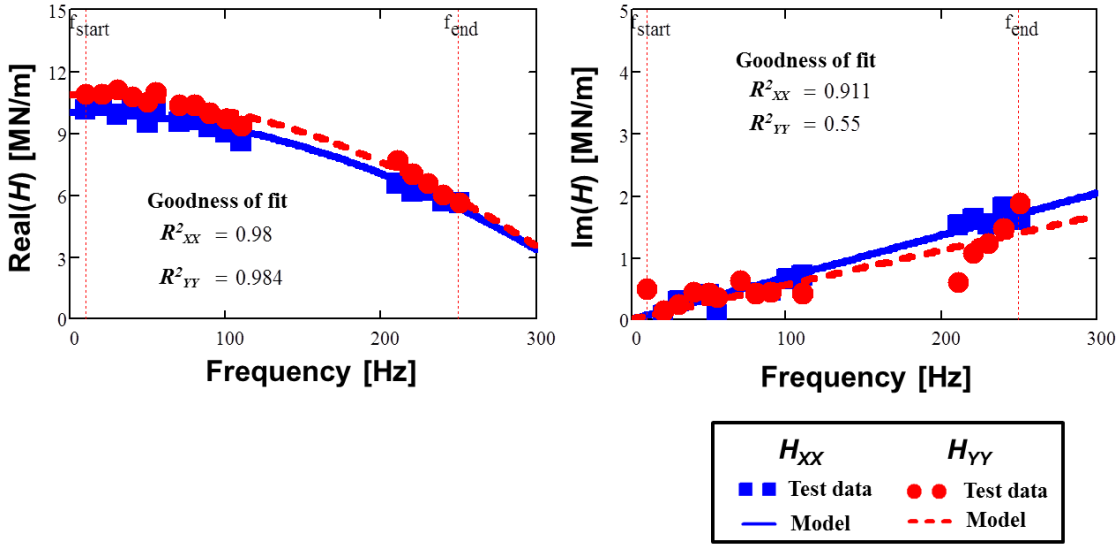

Figure C.3. Dry test system: Real and imaginary parts of the system direct impedances (H_{XX}, H_{YY}) versus excitation frequency. Circular orbit dynamic load tests (without lubricant). Test data and model fits for frequency range 10 Hz to 250 Hz.

Appendix D. Cross-coupled impedances from impact load tests

Figures D.1 and D.2 show the real and the imaginary parts of the cross-coupled dynamic impedances (H_{XY}, H_{YX}) for unidirectional impact load tests with increasing BC peak displacement (Z/c). Note that the frequency range for the respective physical model curve fits spans from f_{start}=10 Hz to f_{end}=300 Hz. The SFD cross-coupled coefficient magnitudes are more than one order smaller than the direct coefficient; hence showing low correlation factor (R^2) to the respective physical model.

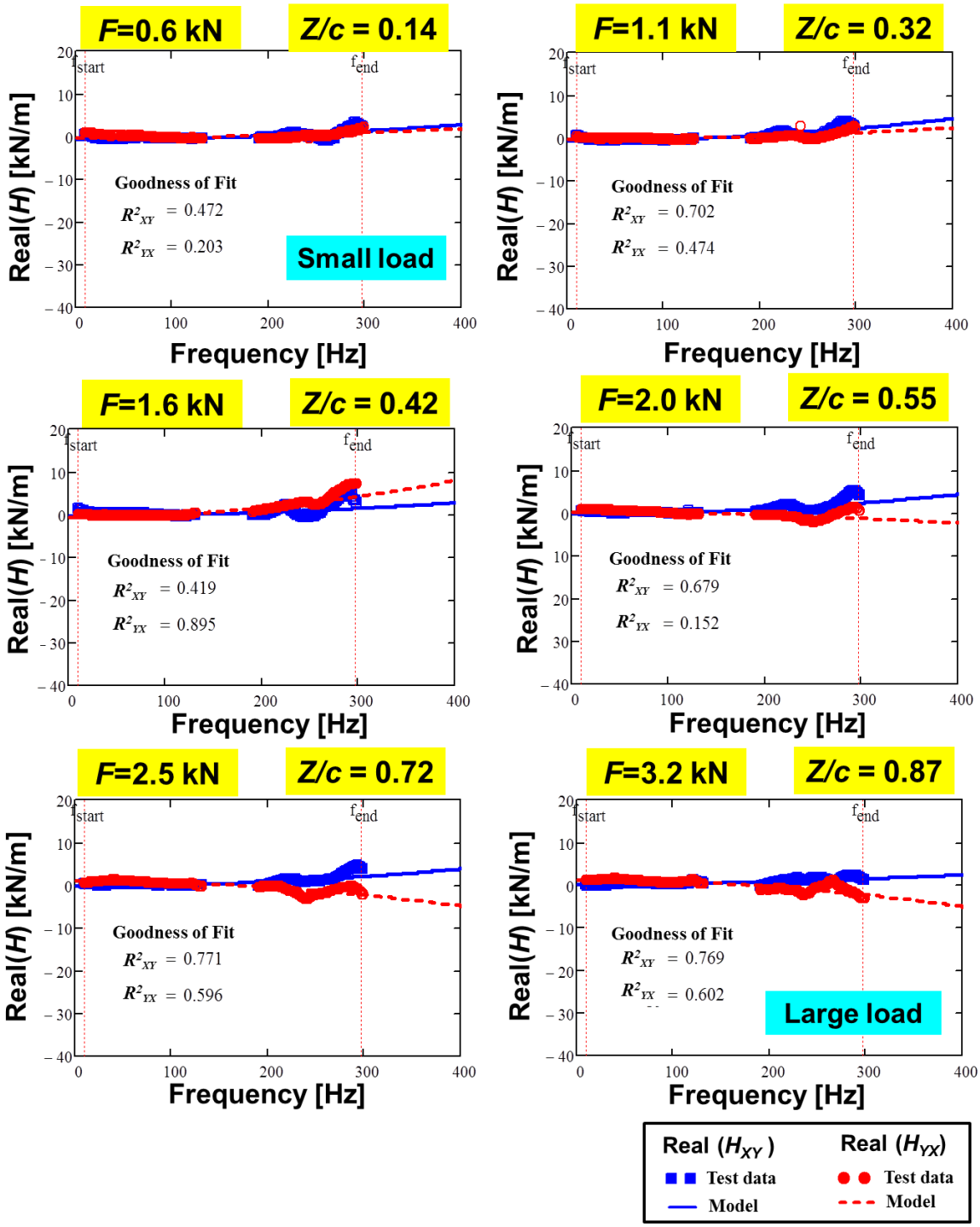

Figure D.1. Real part of the test system cross-coupled impedances (H_{XY}, H_{YX}) versus excitation frequency. Tests with unidirectional dynamic loads (0.5 – 3.2 kN) with BC peak amplitudes Z/c=0.14 - 0.87 and centered condition (e_S=0.0c). Test data and model fits. Open-ends SFD with c=213 μm and 25.4 mm single film lands.

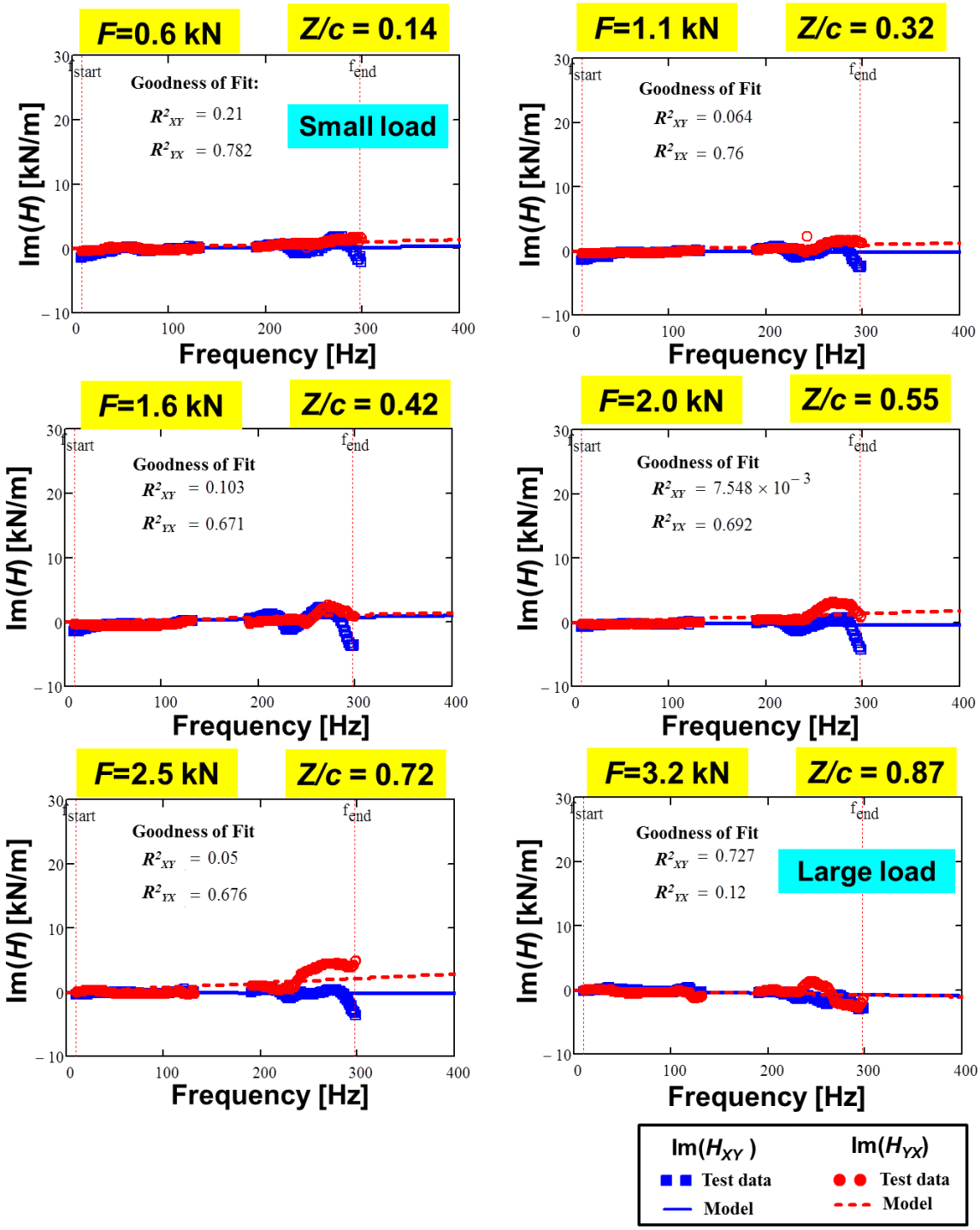

Figure D.2. Imaginary part of the test system cross-coupled impedances (H_{XY}, H_{YX}) versus excitation frequency. Tests with unidirectional dynamic loads (0.5 – 3.2 kN) with BC peak amplitudes Z/c=0.14 - 0.87 and centered condition (e_S=0.0c). Test data and model fits. Open-ends SFD with c=213 μm and 25.4 mm single film lands.

Appendix E. Uncertainty analysis

This section outlines the calculation of uncertainty in identified SFD force coefficients. The total uncertainty consists of a bias (instrument) uncertainty and a precision (measurement variability) uncertainty. Both types of uncertainty are outlined, along with the combination of bias and precision into total uncertainty for each force coefficient $(K, C, M)_{\mathrm{SFD}}$. For brevity the calculated values are based on largest possible cases; the actual uncertainty values may be less than these calculated values. Bias, precision, and total uncertainty denoted as *B*, *P*, and *U*, respectively.

Bias uncertainty

The data acquisition (DAQ) board has a rated uncertainty of $B_{DAQ} = 0.1\%$ in the measurement of voltage [E.1]. The DAQ board sampling rate is 4096 samples/second, storing 4096 samples and giving an uncertainty in the output frequency of $B_{\omega} = 0.5\mathrm{Hz}$ for the entire frequency range [E.1]. This is equivalent to $B_{\omega} = 5\%$ at the lowest frequency of 10 Hz. The uncertainty of *X* and *Y* – REBAM® (displacement) sensors are $B_X = 1.8\%$ and $B_Y = 1.7\%$, respectively. The load cell uncertainty is $B_{LOAD} = 2.0\%$. With these individual uncertainties, the propagation of uncertainty into the measurements of displacement and force, respectively, are

$$B_{DISP} = \sqrt{(B_{REBAM})^2 + (B_{DAQ})^2} = 1.8\% \tag{E.1}$$

$$B_{FORCE} = \sqrt{(B_{LOAD})^2 + (B_{DAQ})^2} = 2.0\% \tag{E.2}$$

Knowledge of frequency domain relations $K \sim F/D$, $C \sim (F/D)\omega$, and $M \sim (F/D)\omega^2$ aids to determine the total bias uncertainty in force coefficients as

$$B_K = \sqrt{(B_{DISP})^2 + (B_{FORCE})^2} = 2.7\% \tag{E.3}$$

$$B_C = \sqrt{(B_{DISP})^2 + (B_{FORCE})^2 + (B_{\omega})^2} = 5.7\% \tag{E.4}$$

$$B_M = \sqrt{(B_{DISP})^2 + (B_{FORCE})^2 + (2 \cdot B_{\omega})^2} = 10.4\% \tag{E.5}$$

Recall, determination of the SFD force coefficient requires subtraction of dry system coefficients from lubricated system coefficients, i.e.

$$(\mathbf{K}, \mathbf{C}, \mathbf{M})_{\mathrm{SFD}} = (\mathbf{K}, \mathbf{C}, \mathbf{M}) - (\mathbf{K}, \mathbf{C}, \mathbf{M})_{\mathrm{S}} \tag{E.6}$$

Therefore, propagation of the bias uncertainty from two measurements into the SFD coefficient's bias is

$$B_{K_{SFD}} = \sqrt{(B_{K_S})^2 + (B_K)^2} = 3.8\% \quad \text{(E.7)}$$

$$B_{C_{SFD}} = \sqrt{(B_{C_S})^2 + (B_C)^2} = 8.0\% \quad \text{(E.8)}$$

$$B_{M_{SFD}} = \sqrt{(B_{M_S})^2 + (B_M)^2} = 14.6\% \quad \text{(E.9)}$$

Precision uncertainty

Precision uncertainty deals with the repeatability of measurements. Plotting the real and imaginary part of the measured impedance versus frequency and using an IVFM curve fit (variation of least squares) gives plots as those shown in Figure E.1. The stiffness coefficient (*K*) is estimated as the *Y*-intercept and the mass coefficient (*M*) is estimated as the curvature of the real part of the measured mechanical impedance. The slope of the imaginary part of the measured mechanical impedance is the estimated damping coefficient (*C*).

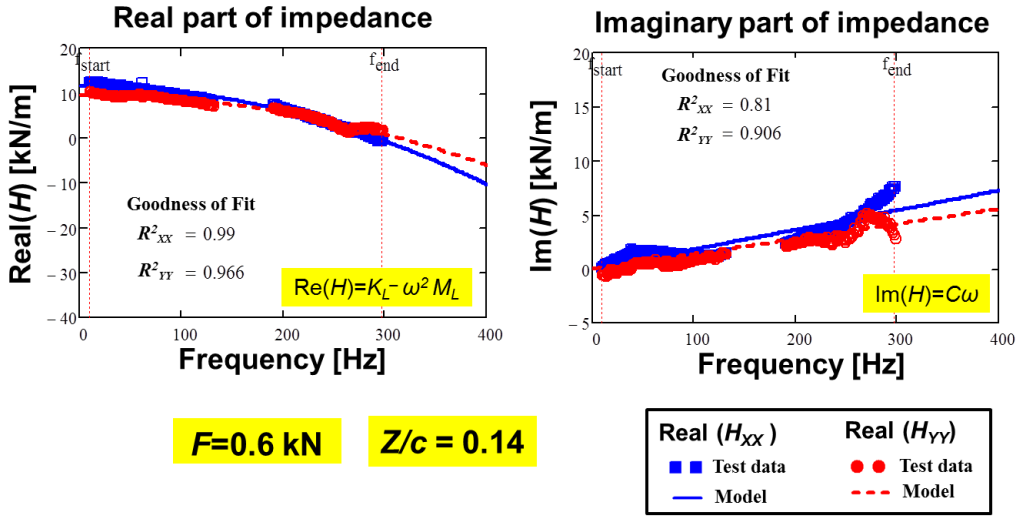

Figure E.1 Plots real (a) and imaginary (b) parts of mechanical impedance versus frequency (*ω*). Curve fit and measured data shown

For the estimation of precision uncertainty for a multiple measurements, Ref. [E.2] gives

$$P = 1.81 \cdot \frac{S}{\sqrt{M}} \quad \text{(E.10)}$$

where S and M are the estimated standard deviation based upon engineering knowledge and the number of multiple tests performed, respectively. Ref [E.3] gives relations for estimated standard deviation of the intercept and slope of a least squares fit line as

$$S_{Intercept} = \sqrt{\frac{1}{N(N-2)}\frac{1-r^2}{r^2}} \tag{E.11}$$

$$S_{Slope} = \sqrt{\frac{1}{(N-2)}\frac{1-r^2}{r^2}} \tag{E.12}$$

where N is the number of points used for the curve fit and r^2 is the curve fit correlation. Using the relations given in E.11 and E.12 with N=240 and r^2=0.95, the propagation into the uncertainty of SFD coefficients gives

$$P_{K_{SFD}} = \sqrt{(P_{K_S})^2 + (P_K)^2} = 0.4\% \tag{E.13}$$

$$P_{C_{SFD}} = \sqrt{(P_{C_S})^2 + (P_C)^2} = 1.0\% \tag{E.14}$$

$$P_{M_{SFD}} = \sqrt{(P_{M_S})^2 + (P_M)^2} = 1.2\% \tag{E.15}$$

Total uncertainty

The total uncertainty in each SFD force coefficients are

$$U_{K_{SFD}} = \sqrt{(B_{K_{SFD}})^2 + (P_{K_{SFD}})^2} = 3.8\% \tag{E.16}$$

$$U_{C_{SFD}} = \sqrt{(B_{C_{SFD}})^2 + (P_{C_{SFD}})^2} = 8.1\% \tag{E.17}$$

$$U_{M_{SFD}} = \sqrt{(B_{M_{SFD}})^2 + (P_{M_{SFD}})^2} = 14.7\% \tag{E.18}$$

References

[E.1] "NI cDAQ – 917x User Manual," User manual for NI CompactDAQ9171/9174/9178 USB Chassis, National Instruments, July 2011, Appendix A. Specifications.

[E.2] Beckwith, T., Marangoni, R., and Lienhard, J. 1993, "Mechanical Measurements", Prentice Hall, 5th edition, pp. 82

[E.3] "Uncertainty Analysis", Physical Chemistry Laboratory, University of Delaware, Accessed Jan. 2013, pp. 9, http://www.udel.edu/pchem/C446/error.pdf